Calcium alginate hydrogel for high-yield adsorption-based desalination driven by ultralow-grade heat

Cell Reports
Physical Science

Article

Calcium alginate hydrogel for high-yield adsorption-based desalination driven by ultralow-grade heat

Graphical abstract

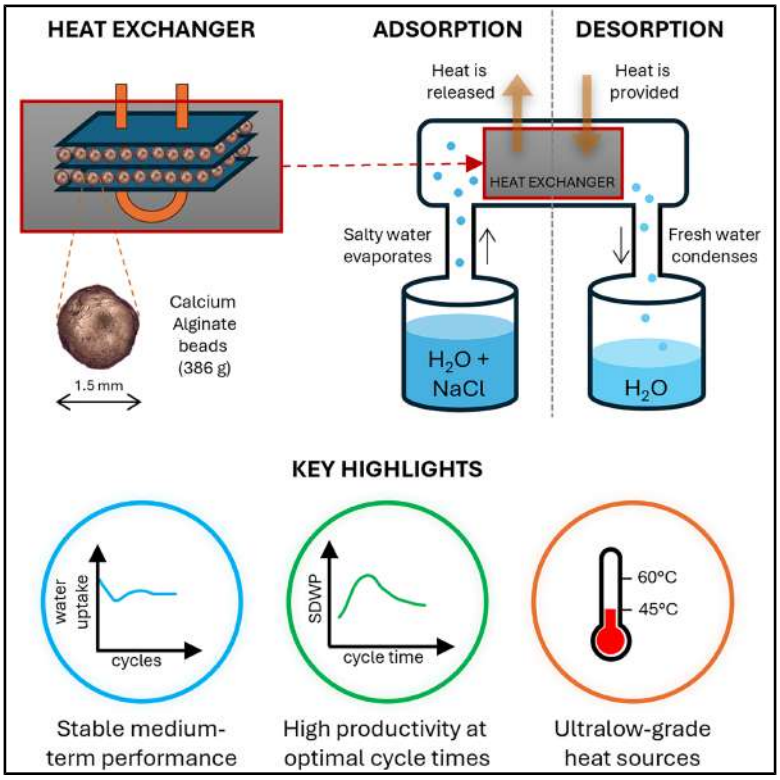

Highlights

- Calcium alginate hydrogel is tested for adsorption-based water desalination
- Stable material performance over 40 cycles of normal operation under vacuum
- An optimal specific daily water production of 6 m^3/day/ton at 60°C is achieved
- Desalination driven by ultralow-grade heat sources at temperatures as low as 45°C

Authors

Matteo Calò, Vincenzo Gentile, Matteo Fasano, Eliodoro Chiavazzo

Correspondence

matteo.calo@polito.it (M.C.), eliodoro.chiavazzo@polito.it (E.C.)

In brief

Adsorption desalination stands out as a promising solution to produce freshwater, leveraging ultralow-grade heat. Calò et al. demonstrate that a bio-derived calcium alginate hydrogel can be used as an alternative to other common sorbents, with stable medium-term performance and water productivity even at temperatures below 60°C.

Calò et al., 2026, Cell Reports Physical Science 7, 103139
March 18, 2026
https://doi.org/10.1016/j.xcrp.2026.103139

CellPress

Cell Reports
Physical Science

CellPress
OPEN ACCESS

Article

Calcium alginate hydrogel for high-yield adsorption-based desalination driven by ultralow-grade heat

Matteo Calò,[1,*] Vincenzo Gentile,[1] Matteo Fasano,[1,2] and Eliodoro Chiavazzo[1,2,3,*]
[1]Department of Energy, Politecnico di Torino, Corso Duca degli Abruzzi 24, Turin, Italy
[2]Clean Water Center, Politecnico di Torino, Corso Duca degli Abruzzi 24, Turin, Italy
[3]Lead contact
*Correspondence: matteo.calo@polito.it (M.C.), eliodoro.chiavazzo@polito.it (E.C.)
https://doi.org/10.1016/j.xcrp.2026.103139

SUMMARY

Adsorbent-based desalination stands out as a promising solution to produce fresh water leveraging on ultralow-grade heat. We investigate the use of a bio-derived calcium alginate (CaAlg) hydrogel, an alternative to other common sorbents. A batch of CaAlg is synthesized and characterized in a gravimetric sorption analyzer. The resulting type II isotherm at 30°C shows an exceptional water uptake equilibrium value of 1.28 g/g at a relative humidity of 70%, realizing nearly a 4-fold increase compared to standard silica gels under the same conditions. We test CaAlg under vacuum in a water desalination unit. Our material shows an excellent medium-term cyclability, with a stable uptake over 40 cycles of operation. We achieve water production even at a temperature as low as 45°C, with a specific daily water production (SDWP) of 6 m^3/day/ton using a hot-source temperature of 60°C, realizing the most performant small-scale system in the context of ultralow-grade waste heat valorization.

INTRODUCTION

Freshwater scarcity is a global problem. The available reserves constitute only 3% of the total water on Earth; they are not uniformly distributed and they are often difficult to access or contaminated. As a result, billions of people in the world suffer from water shortage,[1–4] making desalination a key technology to cope with this issue, especially when seawater is accessible. In this context, the research for new, effective, and sustainable desalination solutions is crucial.

The most common desalination technology is reverse osmosis (RO), a mature technology with elevated cost for installation but with optimized electricity consumption (1.8–5 kWh/m^3) needed to reject over 99% of the solute. However, RO plants require high-exergy sources in order to apply the necessary work to overcome osmotic pressure, requiring additional investment costs in the case of integration with renewable energy.[5,6] On the other hand, thermal desalination technologies have the advantage of requiring lower exergy sources, such as low-temperature heat. Multi-stage flash distillation (MSD) and multiple-effect distillation (MED) belong to this category, and their energy consumptions per cubic meter of water are 60–80 kWh of heat in addition to 1–5 kWh of electrical energy, needed to run auxiliaries of plants.[7,8] Membrane distillation (MD) is an alternative low-cost distillation technique that can be driven with low-exergy heat, with energy consumption between 225 kWh/m^3 and 500 kWh/m^3 of condensed water.[9–12] In adsorption desalination (AD), an emerging thermal technology, a sorbent material is used to drive water vapor from the evaporator (EV) containing salty water to a condenser (CD) with fresh water.[13,14] AD is scalable and, unlike membrane-based technologies, the distillation performance is not impacted by temperature, concentration polarization, and fouling.[15] Furthermore, adsorbent-based solutions are generally environmentally friendly, highly integrable in renewable energy grids (e.g., they can be operated using renewable heat from thermal solar plants[16,17]) and circular-economy viable solutions (they can be operated by using process waste heat[18]). The performances of an adsorption-desalination plant depend strongly on the choice of the adsorbent material: the latter should be sustainable, stable over time, and have large water uptakes and fast kinetics. In this context, the research for new materials is crucial. Conventional AD plants use sorbents such as silica gels, which are typically regenerated at temperatures of 65°C or above.[13] This is a limitation when only lower-grade heat sources are available. In contrast, we propose calcium alginate (CaAlg) as alternative sorbent, a bio-derived adsorbent hydrogel. The material choice is based on the results of previous experimental campaigns,[19] where CaAlg has proved high sorption rates and capacities even when regenerated at temperatures of 60°C or below. In particular, CaAlg has shown an equilibrium water uptake of up to 0.88 g/g (at temperature T = 21°C and relative humidity RH = 47%), larger than ordinary silica gels in similar conditions (0.28 g/g at T = 25°C and RH = 50%[20]). Additionally, we decided to investigate CaAlg for AD because is a bio-derived material and its disposal in case of material replacement comes with a low environmental impact.[21–24] Nevertheless, until now, CaAlg has never been tested under vacuum in an AD unit.

In this research, we characterize experimentally CaAlg, both in a gravimetric analyzer (in comparison with reference microporous and mesoporous silica gels) and under vacuum in a prototypeadsorption-based desalination unit, in particular comparing performances using mesoporous silica gel with the same unit. This allows us to prove that CaAlg has an excellent medium-term cyclability under vacuum, with a stable uptake over 40 cycles of operation. We achieve water desalination at a temperature as low as 45°C, with a specific daily water production (SDWP) of 2.2 m^3/day/ton, higher than silica gel tested under the same conditions. Furthermore, we achieve an optimal SDWP of 6 m^3/day/ton when using a hot-source temperature of 60°C.

RESULTS

Operating principle

In adsorption-based technologies, the separation of water from contaminated liquid solutions is obtained by operating a working cycle based on three consecutive phases: adsorption, desorption, and pre-cooling. First, a vacuum chamber (EV tank) containing the evaporating feedwater is put in communication with a second vacuum chamber (adsorber) containing the sorbent under test. During this phase (adsorption), water vapor evaporates and is physically bonded to material micropores. Then, the communication between the EV tank and adsorber is interrupted, and the desorption process starts. During this phase, increasing the sorbent temperature breaks the physical bonds between the water and the sorbent and the water vapor is released back. The latter condenses on the internal walls of the adsorber vessel, and it is collected from a third vacuum chamber placed at the bottom of the adsorber (CD pipe). Finally, all the chambers are isolated, and the machine is cooled down in preparation for the next cycle (pre-cooling phase).

The choice of a proper heat exchanger is crucial in order for the sorbent material to efficiently exchange both thermal energy and vapor mass with the environment. For this research, we packed the material in a finned coil heat exchanger (Figure 1A) and placed the latter in the adsorber chamber of the desalination unit (Figure 1B). In Figure 1C, we show the schematic of the setup, including the vacuum circuit (blue areas), the external hydraulic circuits exchanging heat with the machine (orange and magenta loops), temperature sensors, pressure sensor, flowmeter, and actuators (details are provided in the methods section).

Material characterization

The material studied in this research is a biopolymeric hydrogel referred to as CaAlg, obtained by crosslinking sodium alginate (NaAlg) (a salt contained in the cell membranes of brown algae[25]) with calcium ions.[26,27] More details on the hydrogel synthesis are reported in the methods section. Figures 1D, E, F, and G show increasingly larger details of CaAlg beads: first, when placed in the heat exchanger; second, under an optical microscope; and third and fourth, under scanning electron microscopy (SEM) imaging.

Figure 2A shows the adsorption and desorption isotherms at 30°C obtained on aged samples of CaAlg (details in the methods section). Vertical bars represent ±3 standard deviations, modeling the uncertainty due to inhomogeneity in the produced samples (negligible in the case of silica gels). Isotherms carried out on silica gel samples (microporous silica gel with grain size 0.5–1.5 mm and mesoporous silica gel with grain size 1.5–3.15 mm) are also plotted for reference. At the RH of 70%, the CaAlg reaches an uptake of 1.28 g/g, while the microporous and mesoporous silica gel reach uptakes of 0.29 and 0.34 g/g (about 4 times smaller). Furthermore, the CaAlg isotherm shows higher linearity and less hysteresis. Given the reversed "S" shape, the CaAlg isotherm can be classified as "type II" according to the ISO classification.[28] Thus, the Guggenheim-Anderson-DeBoer model (GAB)—a variation of the Brunauer-Emmett-Teller (BET) model—can be used to best-fit the curve[28,29]:

$$w = \frac{w_m \cdot c \cdot K \cdot RH}{(1 - K \cdot RH) \cdot (1 + (c - 1) \cdot K \cdot RH)} \quad \text{(Equation 1)}$$

where w_m is the monomolecular layer uptake, RH is relative humidity, K is a corrective coefficient extending BET validity, and c is the original BET coefficient. The latter can be written as a function of the enthalpy of the adsorption process H_{ads}, latent heat of evaporation of water H_{liq} (equal to 2430 kJ/kg at 30°C[30]), universal gas constant R = 8.315 $J/(mol \cdot K)$, and absolute temperature T, according to Equation (2):

$$c = e^{\frac{H_{ads} - H_{liq}}{RT}}, \quad \text{(Equation 2)}$$

The resulting curve, best-fitted on the adsorption isotherm, is shown in Figure 2A (black dotted line). The values w_m = 0.7317g/g, c = 3.4558, and K = 0.7704, resulting from the best-fitting procedure, are physically consistent, being w_m below the maximum capacity, K between 0 and 1, and c greater than 2 (which is consistent with a type II isotherm).[31] By inverting Equation (2), the enthalpy of adsorption can be estimated to be 2,600 kJ/kg. This value is approximately 7% larger than the latent heat of evaporation for water at 30°C. If compared with literature, this is close to the values for silica gels and slightly lower than metal organic frameworks (MOFs) (see also Tables S1 and S2 in Note S1). Figure 2B shows the adsorption equilibrium values of samples of CaAlg after 0, 20, 30, and 40 aging cycles in the desalination unit. The values after the first 20 cycles are, in the RH range between 40% and 70%, from 5% to 10% lower than the isotherm of the material "as produced." This can be explained by the material not being perfectly dry after the production process (see also Figure S1 in Note S2). Using X-ray diffractions,[32] authors have demonstrated that initial dehydration of the hydrogel (the first responsible for the loss of "composition water") induces the formation of secondary junction zones among functional groups with un-crosslinked Ca cations. These junctions among parallel alginate chains are strong enough to be preserved also on successive rehydration of the hydrogel once it is exposed to moisture. However, the process of losing the composition water is not completed with one single dehydration and continues during the first thermal cycles. The progressive reduction in dry mass during the first cycles due to this aspect is visible in the initial drop of the equilibrium moisture uptake. After this initial drop, though, the equilibrium values stabilize. The convergence of the material's behavior is coherent with what is observed for CaAlg samples in the literature.[33] Figure 2C compares the CaAlg adsorption isotherm at 30°C (vertical bars represent ±3 standard deviations)

Please cite this article in press as: Calò et al., Calcium alginate hydrogel for high-yield adsorption-based desalination driven by ultralow-grade heat, Cell Reports Physical Science (2026), https://doi.org/10.1016/j.xcrp.2026.103139

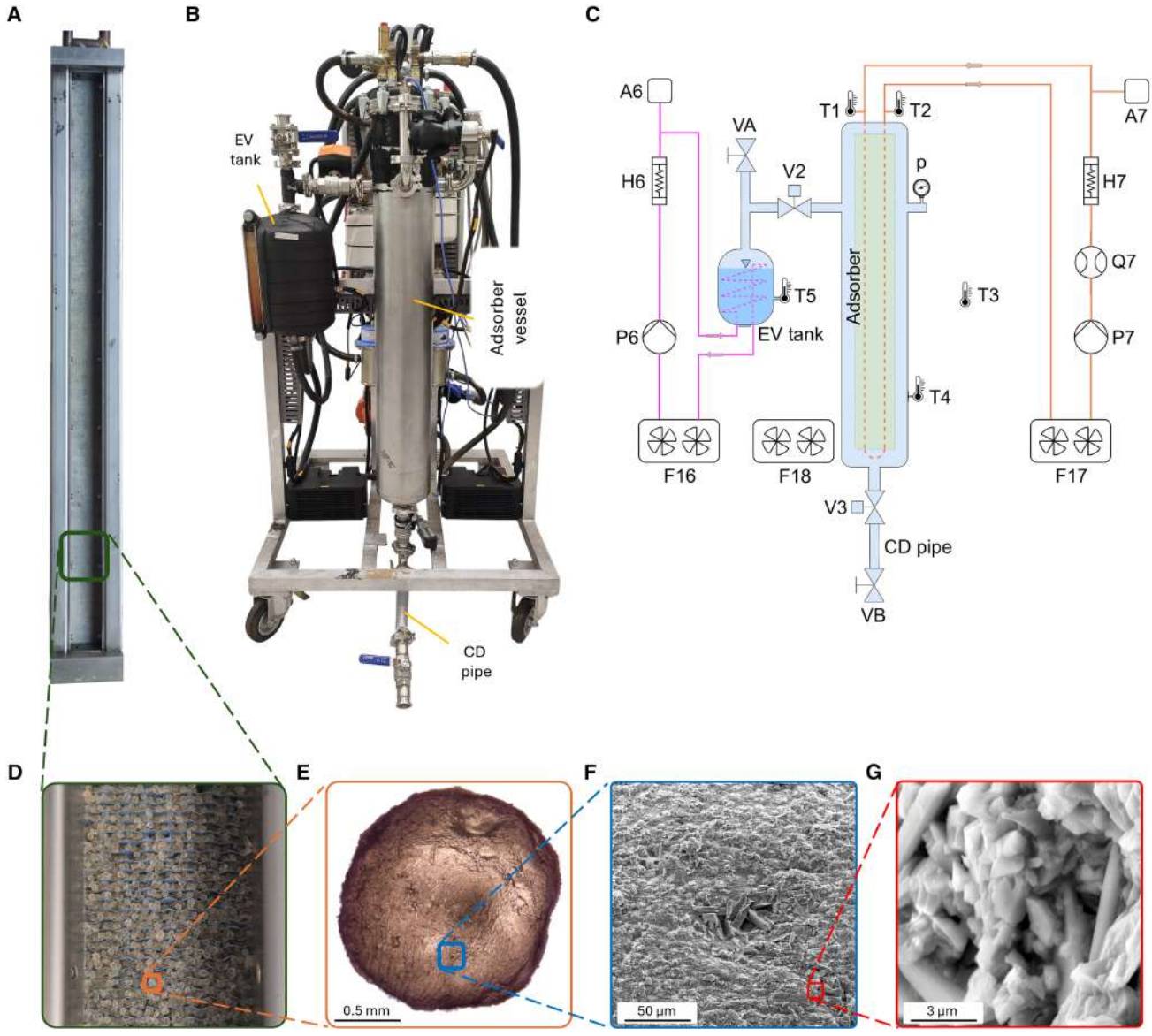

Figure 1. Single-bed adsorption desalination unit

(A) Heat exchanger containing the sorbent material under test.

(B) Desalination unit. The evaporator (EV) tank contains the feedwater; the adsorber vessel contains the heat exchanger filled with the sorbent material; and the condenser (CD) pipe collects the desalinated water.

(C) Schematics of the desalination unit, showing the vacuum circuit (blue areas), the external pressurized circuit exchanging heat with the adsorber (orange), and the external pressurized circuit exchanging heat with the EV tank (magenta). The unit is provided with temperature sensors (T1, T2, T3, T4, and T5), a pressure sensor (p), a flowmeter (Q7), four valves (V2, V3, VA, and VB), two pumps (P6 and P7), three dry-coolers (F16, F17, and F18), two electric heaters (H6 and H7), and safety accessories (A6 and A7).

(D) Detail of the heat exchanger, where the 3-mm-large spaces among the fins are filled with CaAlg beads.

(E) Zoom on a single bead of CaAlg under a 5× optical lens, with backlighting. Scale bars, 0.5 mm.

(F) A SEM image with magnification 1,000× of the surface of a bead of CaAlg. Scale bars, 50 µm.

(G) A SEM image with magnification 20,000× of the surface of a bead of CaAlg. Scale bars, 3 µm.

with results from the literature.[34–39] For relative humidities higher than 20%, the aged CaAlg sample has the highest equilibrium water uptake, except in the range 45%–65% where it is outperformed by a modified MIL-101 MOF. The shape of the isotherm and high linearity are consistent with the results on the CaAlg sample from the literature.[34] MOFs, such as MOF-801, are competitive at low RH values (below 20%). Figures 2D and 2E show pictures of the significant samples tested in this research, respectively: CaAlg "as produced" (no aging cycles), CaAlg after 40 aging cycles, microporous silica gel, and mesoporous silica gel.

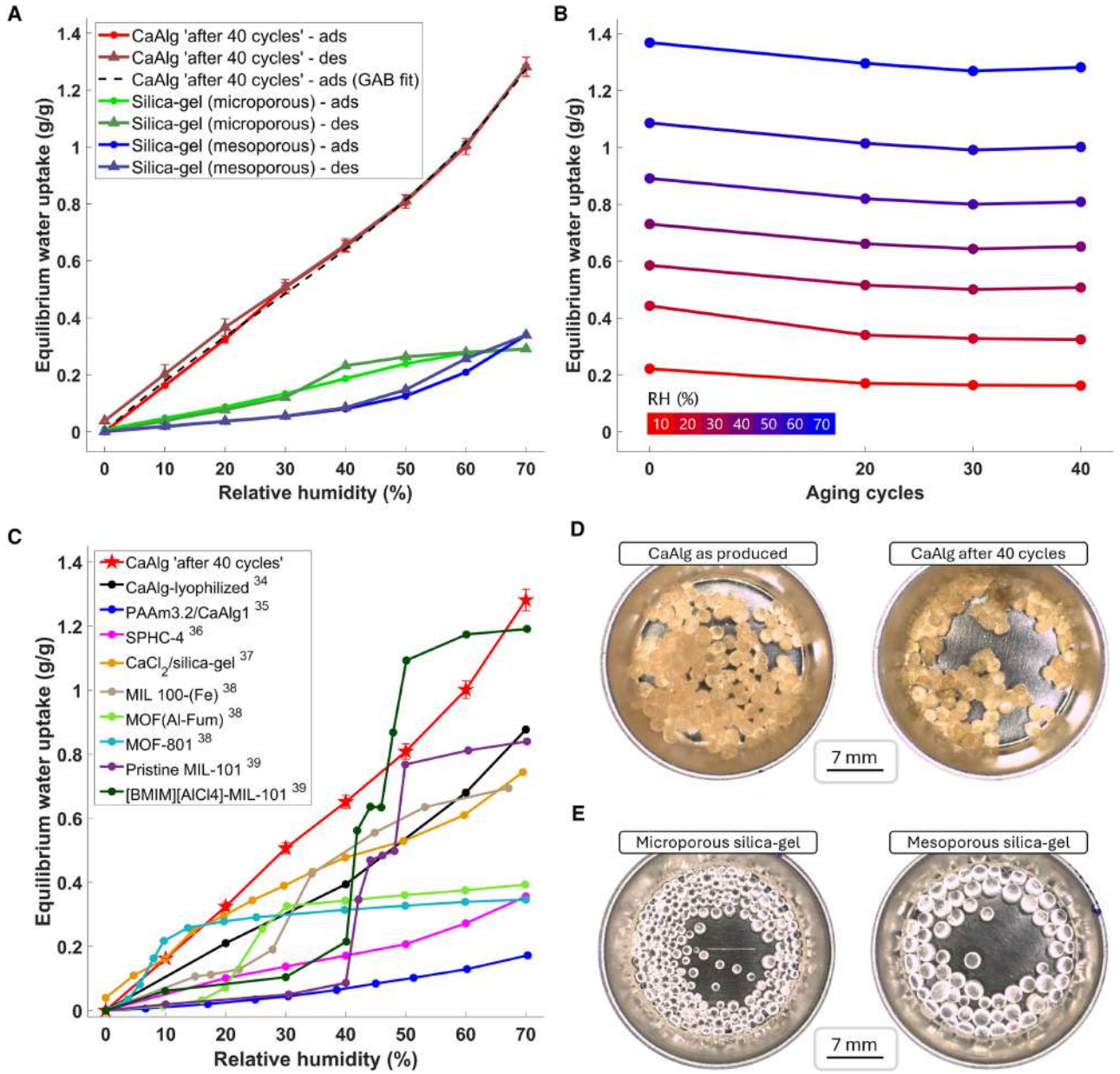

Figure 2. Material characterization: Isotherms and aging

(A) Isotherm at 30°C of CaAlg after 40 cycles of testing, compared with microporous and mesoporous reference silica gels. Both adsorption (ads) and desorption (des) ramps are shown. Vertical bars represent ± three standard deviations. The Guggenheim-Anderson-DeBoer (GAB) best-fitting curve on the CaAlg adsorption ramp is plotted in comparison.

(B) Equilibrium values at different relative humidities for samples that underwent 0, 20, 30, and 40 cycles of testing.

(C) Adsorption isotherm at 30°C of CaAlg in comparison with materials from the literature. Vertical bars represent ± three standard deviations.

(D) Samples of CaAlg as produced and after 40 cycles of testing, in equilibrium at temperature T = 30°C and relative humidity RH = 40%. Scale bars, 7 mm.

(E) Samples of microporous and mesoporous silica gel, in equilibrium at T = 30°C and RH = 40%. Scale bars, 7 mm.

Cycling CaAlg in the desalination unit

Figure 3A shows the resulting trends of the monitored thermodynamic variables when CaAlg is cycled in the desalination unit (details in the methods section). The test consists of 6 consecutive cycles, each composed of the adsorption phase ADS (30 min with the target adsorption temperature of 30°C), the desorption phase DES (45 min with the target desorption temperature of 60°C, in this case), and the pre-cooling phase PC (15 min). The three phases are highlighted in the first cycle of Figure 3A and repeat identically for 9 h. At the beginning of the ADS phase, temperature T2 (outlet of the adsorber) is greater than temperature T1 (inlet of the adsorber), consistent with

Please cite this article in press as: Calò et al., Calcium alginate hydrogel for high-yield adsorption-based desalination driven by ultralow-grade heat, Cell Reports Physical Science (2026), https://doi.org/10.1016/j.xcrp.2026.103139

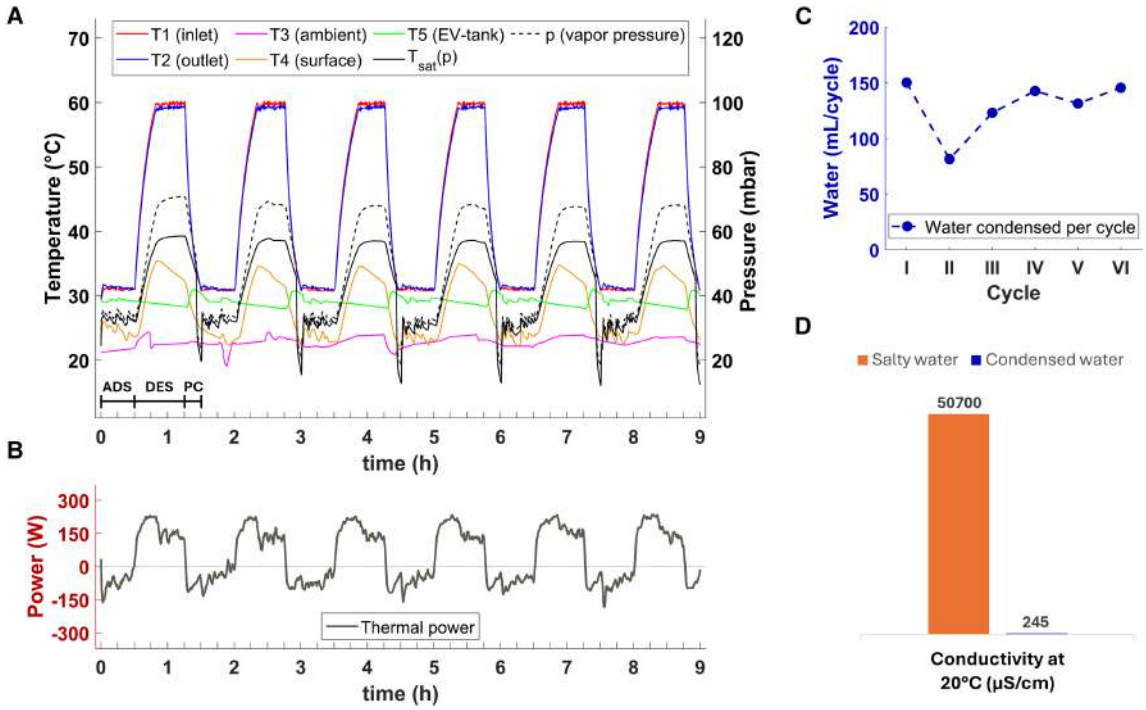

Figure 3. Cycling CaAlg in the desalination unit

(A) 1-day test using CaAlg in the desalination unit. The test consists of 6 consecutive cycles, each of which is composed of adsorption phase ADS, desorption phase DES, and pre-cooling phase PC, as highlighted in the first cycle. Temperatures T1 (inlet of the adsorber), T2 (outlet of the adsorber), T3 (ambient), T4 (vessel surface), T5 (evaporating water), and T_{sat} (saturation temperature at the vapor pressure in the adsorber) are shown on the left axis as a function of test time; vapor pressure p is shown on the right axis.

(B) Thermal power (positive when absorbed by the adsorber) is shown as a function of test time. It is evaluated as the product of the external circuit's water density ρ, flow rate Q, specific heat c_p, and the temperature difference (T1 - T2).

(C) Water collected in the CD pipe at the end of each of the six cycles.

(D) Conductivity of water at 20°C before and after the desalination process.

adsorption being an exothermic process. The opposite is true during desorption, the latter being an endothermic process.

The heating transient in the first 20 min of the desorption phase is necessary to overcome the thermal inertia of the system and bring the adsorber to the target desorption temperature. The pressure p during desorption increases during the heating process and decreases slightly during the rest of the phase, while condensation happens in the adsorber. The saturation temperature T_{sat} is evaluated at pressure p using the Antoine equation.[40] From Figure 3A, T_{sat} follows qualitatively the temperature T4 (external surface of the adsorber vessel), which is consistent with the condensation process.

Figure 3B shows the thermal power exchanged with the adsorber (uncertainty propagation is discussed in Note S3). This is positive during desorption and negative during adsorption and pre-cooling, which is consistent with the nature of the processes. Figure 3C shows the water production at the end of each of the 6 cycles; after initial oscillations in the first 2 cycles, the production stabilizes. This occurs because the chosen adsorption and desorption times initially prevent the material from returning to its starting uptake values. Keeping on cycling, the cycle converges toward a range of uptakes that is compatible with the chosen parameters. This behavior is consistent across various conditions and supported by the literature.[41]

The results of the experimental campaign under all tested conditions are found in Note S4 (Table S3; Figures S2-S10).

In Figure 3D, we show the results of a water analysis (see methods section) conducted on samples collected from the desalination unit. A desalination effect was indeed achieved: we started from feedwater with the salinity level comparable with seawater (conductivity of 50700 µS/cm) and produced water with a conductivity of 245 µS/cm at 20°C. For reference, the World Health Organization[42] suggests for drinkable water, a limit of total dissolved solids equal to 600 mg/L, corresponding to approximately 900 µS/cm at 20°C.[43] Nevertheless, some salt is still present in the condensed water. This can be explained by aerosol migrating from the EV into the adsorber (see also Figure S11, in Note S5). The complete list of results of the analyses performed on the water samples is reported in Supplementary 6 (Table S4; Figures S1–S13).

Desalination plant performance

Figure 4A shows the specific water production (i.e., the amount of condensed water divided by the amount of dry sorbent) achieved with the desalination unit at different desorption temperatures (vertical bars represent ±1 standard deviation). The curves obtained with CaAlg and mesoporous silica gel are shown for comparison, proving that CaAlg can reach specific

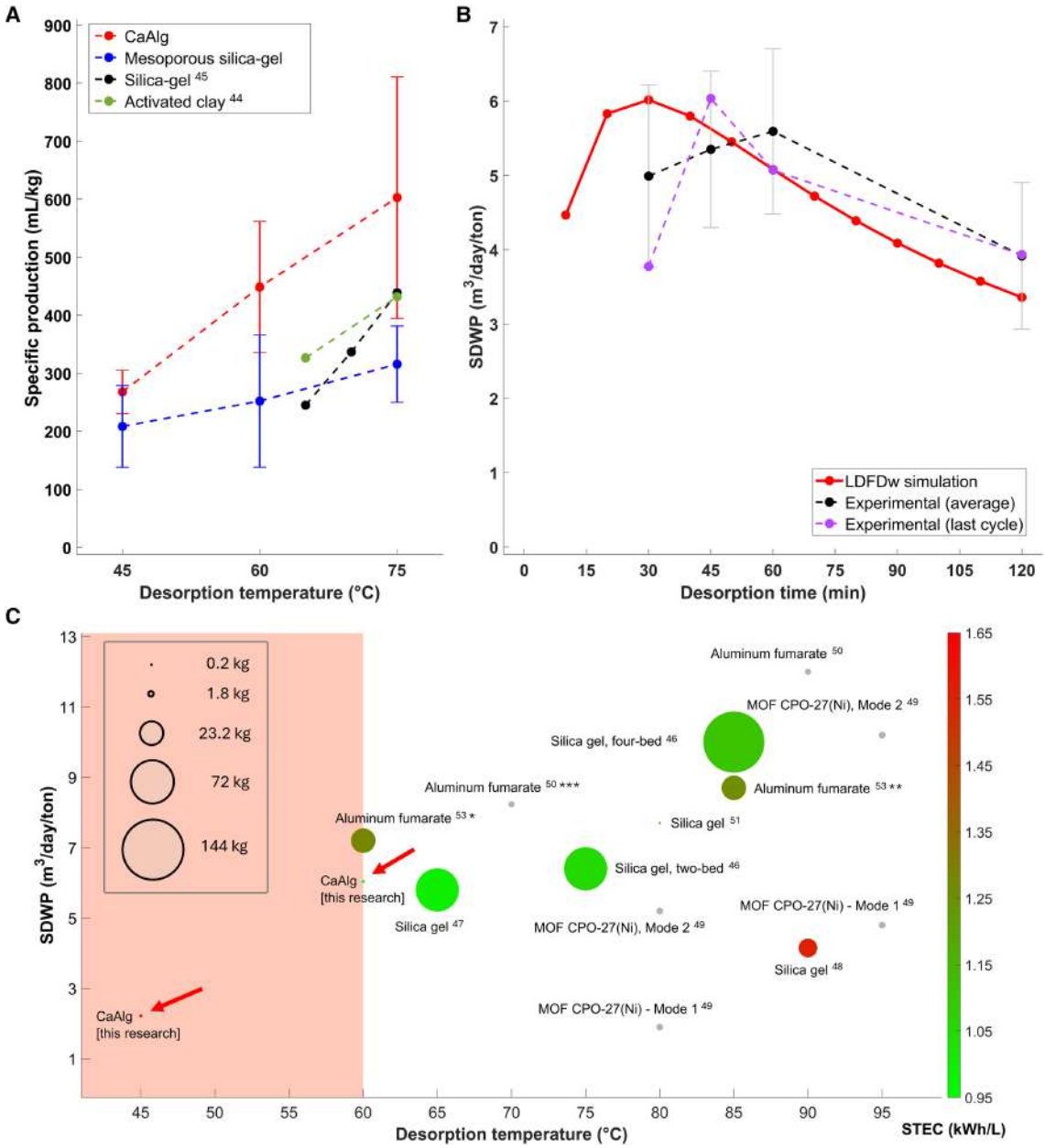

Figure 4. Performance of the desalination plant

(A) Specific water production as a function of test desorption temperature. Experimental results for CaAlg and mesoporous silica gel are shown, as achieved in the desalination unit with the adsorption time of 30 min, adsorption temperature of 30°C, and desorption time of 120 min. Vertical bars indicate ± one standard deviation. Results achieved with different plants from the literature are shown in comparison.

(B) Specific daily water production (SDWP) as a function of test desorption time. Experimental results for CaAlg are shown, as achieved in the desalination unit with the adsorption time of 30 min, adsorption temperature of 30°C, and desorption temperature of 60°C. The graph contains the experimental SDWP evaluated considering the average production of the day (black, with vertical bars indicating ± one standard deviation), the experimental SDWP evaluated considering the production from the last cycle of the day (purple), and the theoretical SDWP simulated through the model LDFDw.

(C) Map showing the performance of the desalination unit in comparison with adsorption-desalination plants from the literature. SDWP is shown as a function of desorption temperature. The dot's color shows the needed specific thermal energy consumption (STEC). The dot's area is proportional to the amount of sorbent in the plant. The ultralow-grade heat region for temperatures below 60°C is colored in orange. All reported plants use a CD temperature between 25°C and 30°C, except for * (20°C) and for our plant (23°C). All reported plants use an EV temperature between 27°C and 30°C, except for ** (24°C) and *** (20°C).

Please cite this article in press as: Calò et al., Calcium alginate hydrogel for high-yield adsorption-based desalination driven by ultralow-grade heat, Cell Reports Physical Science (2026), https://doi.org/10.1016/j.xcrp.2026.103139

productions up to 90% larger than silica gel in the same test conditions. For these tests, we fixed adsorption time and temperature (30 min and 30°C, respectively) and desorption time (120 min). In the same picture, results from the literature are shown in comparison.[44,45] The dependence of the SDWP (see methods section) on the cycle time is shown in Figure 4B, where the black curve is experimentally derived considering the average production per cycle (vertical bars represent ±1 standard deviation), while the purple curve refers to the production of the last cycle of the test. For this analysis, we fixed adsorption time and temperature (30 min and 30°C, respectively) and desorption temperature (60°C). We found that an optimal SDWP of 6.04 m^3/day/ton can be achieved at an intermediate desorption time of 45 min.

We used the analytical model "LDFDw", a variation of the linear driving force model "LDF" (where "D" and "w" stand for "Diffusivity" and "water uptake", respectively)[19] to best-fit the charging and discharging transient of the CaAlg (see Figure S14 in Note S7) and found that the diffusivity at 30°C can be estimated as a function of water uptake w as: $D_{30°C} = a+b \cdot w$, with $a = 4.4399 \cdot 10^{-12} m^2/s$ and $b = -2.2985 \cdot 10^{-12} m^2/s$. The estimated diffusivities for all samples are provided in Note S7, Table S5. Starting from this result, we simulated adsorption-desorption transient processes and derived the red curve in Figure 4B (see methods section for details). The result is close to the experimental outcome, except that the latter is right-shifted. This can be explained by the fact that approximately 20 min are needed at the beginning of each desorption phase to bring the adsorber to the target temperature, due to the large thermal inertia of the prototype, meaning that the effective desorption time is shorter than the nominal one.

In Figure 4C, we compare the SDWP and the specific thermal energy consumption (STEC, see methods section) of this research with other adsorption-desalination plants from the literature.[46–53] Most of the plants use high-temperature sources (70°C–95°C), with some of them reaching SDWP above 10 m^3/day/ton; this research, on the other hand, is among the most performant at temperatures below 65°C. This is true especially for the test at 60°C, where desorption time was optimized and the SDWP was maximized (Figure 4B); also, the STEC (0.97 kWh/L) is the lowest, comparable with the ones of the most efficient plants. The temperature range below 60°C is here highlighted and referred to as "ultralow-grade heat" range, based on an expression proposed in Luberti et al.,[54] and it is of particular importance given that most of the waste heat coming from the energy sector (especially coal and nuclear plants) is rejected in such temperature interval and in particular between 40°C and 59°C.[54]

DISCUSSION

We propose CaAlg hydrogel as a sorbent material for high-performance adsorption-based water desalination. We experimentally observed that the CaAlg shows an SDWP of up to 6.04 m^3/day/ton under optimal cycle times (30 min adsorption at 30°C, 45 min desorption at 60°C) in a prototypal desalination unit. When compared with other existing plants, this value is among the largest in the temperature range below 65°C, being only surpassed by the best large-scale solutions using aluminum fumarate with the same hot-inlet temperature and a lower condensation temperature. The estimated STEC of 0.97 kWh/L is the lowest among the analyzed plants, indicating a high thermal efficiency despite the small scale of the unit (less than 1 kg of the sorbent).

Importantly, we achieved a sub-optimal water production even with a desorption temperature as low as 45°C (SDWP of 2.2 m^3/day/ton): this makes the integration of adsorption-based solutions using CaAlg with the power sector an interesting option. Other applications of special interest include data center cooling, where CPU and GPU racks are becoming progressively denser and more energy consuming.[55] In this context, AD employing CaAlg allows combined data center cooling plus desalination. For example, assuming a 500 kW data center cooled via two-phase immersion (fluid temperature of up to 50°C[56]), we can expect to drive an AD plant with the rejected heat and potentially produce up to 12 m^3 of fresh water per day.

We derived experimentally the CaAlg isotherm at 30°C. When plotted in comparison to other sorbents from literature, such as silica gels, MOFs, and other hydrogels, the CaAlg shows larger uptake values (up to 1.28 g/g), higher linearity, and lower hysteresis. The type II resulting isotherm is well modeled by the GAB model, from which an adsorption enthalpy of 2600 kJ/kg was estimated for the hydrogel. The diffusion coefficient during the adsorption process at 30°C and RH = 50% was estimated to be approximately $3 \cdot 10^{-12} m^2/s$. This value is more than three times lower with respect to mesoporous silica gel ($1 \cdot 10^{-11} m^2/s$); this means that silica gel allows to perform more cycles in a given amount of time, and might still be a competitive alternative to CaAlg when short cycles can be performed. Future research should include comparing the SDWP achieved by CaAlg and silica gel undergoing short cycles.

We performed tests using a starting feedwater solution with a conductivity close to seawater. The water condensed by the machine in this case has been analyzed, and a desalination effect was indeed achieved, with a salt rejection rate of over 99.2%.

The material medium-term stability is particularly promising and it was assessed by comparing isotherms on CaAlg samples after they underwent 0, 20, 30, and 40 cycles under the real working conditions in the desalination unit. The demonstrated durability of CaAlg, combined with its biodegradability,[24] make the hydrogel a sustainable and environment-friendly alternative to traditional sorbents. Future research should include extending the analysis to more cycles, in order to check even longer-term stability.

METHODS

Materials preparation

For this research, a batch of 386 g of CaAlg was produced. The polymerization (ionotropic gelation[33,57]) was obtained by dripping a solution of NaAlg (from supplier Carlo Erba Reagents) and water 1% w/w into a solution of $CaCl_2$ and water 8% w/w. The chemicals' concentrations have been chosen based on previous research.[19] The composition of the hydrogel induces variation of moisture capacity and diffusivity: lower levels of NaAlg and higher amounts of $CaCl_2$ enhance the equilibrium water

Please cite this article in press as: Calò et al., Calcium alginate hydrogel for high-yield adsorption-based desalination driven by ultralow-grade heat, Cell Reports Physical Science (2026), https://doi.org/10.1016/j.xcrp.2026.103139

uptake. The introduction of additional elements can further push performances in a specific direction. For example, the addition of micronized graphite induces faster desorption kinetics while decreasing the moisture capacity. Further details on the effect of $CaCl_2$ on bead volume and porosity and on the production setup built to synthesize the material are provided in Note S8 (Figure S15). The resulting beads of CaAlg have a grain size of approximately 1.5 ± 0.1 mm and a density of approximately 2000 ± 400 kg/m^3. For comparison, we purchased and tested microporous and mesoporous silica gels from supplier Oker-Chemie. The mesoporous silica gel has a grain size of 1.5–3.15 mm, and a total of 530 g was placed in the exchanger. The amounts of CaAlg and silica gel were measured after drying in a ventilated oven at 75°C for 12 h. The picture in Figure 1E was obtained using an OPTIKA B-383MET optical microscope. The images in Figures 1F and 1G were obtained using a Quanta 200 FEG environmental SEM.

Desalination unit description

The prototype used to test CaAlg and silica gel for desalination is a single-bed desalination unit from the German company Sorption Technologies GmbH (Figures 1B and 1C). The main vacuum circuit of the machine (blue areas in Figure 1C) consists of the EV tank and a stainless steel and vacuum-proof container of around 5 L, containing the water to be treated; the adsorber vessel (adsorber), a stainless steel, and vacuum-proof cylinder (approximately 20 cm diameter and 100 cm length) contains the heat exchanger filled (Figure 1A) with the adsorbent material under test; the CD pipe, a vacuum-proof reinforced plastic pipe (approx. 400 mL) positioned at the bottom of the machine. A temperature sensor T5 is placed in the vacuum circuit, submerged in the feedwater in the EV tank. In the adsorber, a pressure sensor is placed: this measures the absolute total pressure p around the sorbent, which, when no air or other gases are trapped in the machine, corresponds to the vapor pressure and can be used for later considerations (the machine was checked for leakages and no significant ones were found). The vacuum pressure during a test ranges between 10 and 80 mbar, depending on the test conditions and on the cycle phase. A second circuit in the machine (orange loop on the right in Figure 1C), consisting of an external pressurized hydraulic closed loop moving water at 1.5 bar, is used to transfer thermal energy to the sorbent during the desorption phase and extract energy from the sorbent during the adsorption phase. The copper pipes exchange heat with the material through the exchanger fins. Two temperature sensors T1 and T2 are placed in this circuit, respectively, at the inlet and outlet of the exchanger. A flowmeter Q7 is placed in the circuit: the flow rate was found to be constant during the tests and equal to 3.4 L/min (with an uncertainty of ±0.2 L/min). A pump P7 provides the necessary flow rate. An electric heater H7 and a small dry cooler F17 are used to control the temperature of the water in the loop, in the range 25°C–80°C, according to the needs. The electric heater H7 plays an important role since it simulates the thermal load that, in a real application, is provided by a low-exergy thermal source (e.g., solar panels, low-temperature process waste heat, and so on). The implemented control logic activates the heater whenever the T1 temperature is more than 1°C below the set adsorber temperature. The dry cooler F17 is used for heat dissipation into the environment; it runs whenever the T1 temperature is more than 1°C above the set adsorber temperature. Since there is no buffer tank, but only heater and dry-cooler to act on the water temperature, 15–20 min are necessary for the machine to work against the thermal inertia of the system (the adsorber vessel and exchanger together weight 23 kg in total, most of which is stainless steel AISI-316) and bring the adsorber temperature up to the desired value at the beginning of each working phase. A third circuit (the magenta hydraulic loop in Figure 1C) is used to control the temperature of the feedwater in the EV tank. This loop circulates pressurized water at 1.5 bar and contains similar components as the previous circuit: a pump P6, an electric heater H6, a dry cooler F16, and the necessary safety accessories A6. Unlike the previous circuit, it is not provided with any temperature sensors or any flowmeter; nevertheless, the flow can be reasonably estimated to be the same as in the other circuit (3.4 L/min), given the similar geometry and since the pumps and all the other components are identical. The temperature T5 is used as a feedback value for the temperature control: H6 will heat up the circuit water until T5 is more than 1°C below the set value for the adsorption temperature and F16 will start when T5 is more than 1°C above the same value. Finally, since the condensation process on the adsorber vessel's walls is exothermic and such heat must be dissipated, a further dry cooler F18 has been positioned next to the vessel: by blowing air at 1.42 ± 0.24 m/s (average and standard deviation on 6 measurements at the vessel surface, taken with an anemometer Testo 410i 729), it helps in cooling the vessel walls. In order to monitor such temperature, a sensor T4 has been installed in contact with the vessel's external surface, on the opposite side with respect to F18. A further temperature sensor T3 is positioned at the center of the machine frame, distant from pipes, heaters, and fans, and used to measure the room air temperature. The complete list and description of components, including sensors' accuracies, is provided in Note S9 (Table S6).

Material characterization with a gravimetric sorption analyzer

The sorption materials have been characterized using a gravimetric vapor sorption analyzer from supplier ProUmid, model SPSx-1 μm High Load, with a weighting resolution of 1 μg and reproducibility of ±5 μg. The analyzer allows parallel testing of 23 different samples under a temperature between 20°C and 40°C and a RH between 10% and 70%. Note that the ProUmid analyzer performs the tests under positive pressure (nitrogen is injected in the chamber to control the relative humidity), while the desalination unit works under vacuum; thus, the resulting charging and discharging transients might be characterized by a different diffusivity or equilibrium values. We used the ProUmid analyzer to measure the adsorption and desorption isotherms of the samples at a temperature of 30°C and in the RH range 10%–70%. During this test, the material is kept at 30°C; the RH is gradually increased from 10% to 70% with 10%-step ramps, then decreased back from 70% to 10% with 10%-step ramps. Each RH ramp lasted until the equilibrium condition was satisfied for all samples: according to the settings on the ProUmid analyzer software, a sample is considered in

Please cite this article in press as: Calò et al., Calcium alginate hydrogel for high-yield adsorption-based desalination driven by ultralow-grade heat, Cell Reports Physical Science (2026), https://doi.org/10.1016/j.xcrp.2026.103139

equilibrium when its mass variation with respect to its initial mass in the last 40 min has been below 0.05%. During this test, the machine takes a mass measurement once every 15 min and takes a picture of the sample once in each equilibrium condition. Samples of CaAlg and the reference microporous and mesoporous silica gel have been tested. All the samples are preconditioned in a ventilated oven at 75°C for 12 h before starting the procedure. More details on the experiments and the samples are reported in Note S10 (Figure S16; Table S7). The ProUmid analyzer measures the change in a sample's absolute net mass (m) over time, enabling the calculation of water uptake (w), a key indicator of the material's adsorption performance, defined as follows:

$$w(t) = \frac{m(t) - m_0}{m_0} \quad \text{(Equation 3)}$$

where m_0 is here the lowest value of mass of the material during the test. Given that the ProUmid analyzer has never been used below RH = 10%, the m_0 value is the net mass of the sample in equilibrium in such conditions. In order to compare the collected isotherm with curves from literature and theoretical models, we added an offset to the curves: the isotherms were indeed evaluated assuming the sample mass at RH = 10% as "dry-mass," which means that the uptake is null by definition at RH = 10% for all the curves. In the literature, available models and experimental isotherms assume w = 0 g/g when RH = 0%, which is a condition not achieved in this experimental campaign. For this reason, the CaAlg isotherms were linearly extrapolated outside of the experimental range (the implications of this choice are discussed in Note S11, Figure S17), and the resulting "adjusted" adsorption isotherm is discussed in Figures 2A, B, and C. The GAB model has been used to best-fit the CaAlg isotherm. The GAB model is a generalization of the common BET model, where a third parameter K is added to extend the best-fitting validity to a larger RH range (the BET is usually a valid best-fitting model for RH below 30%).[28,29] The parameter K is defined in such a way that for $K = 1$ the GAB model coincides with the original BET model. The expression used for the GAB model is given in Equation (1).

Two theoretical expressions have been used to model the material change in water uptake over time. The first one is the LDF model[58,59]:

$$w(t) = w_0 + (w_{eq} - w_0)\cdot\left(1 - e^{-\frac{F_0 \cdot D}{R_p^2}t}\right) \quad \text{(Equation 4)}$$

where t is time, w_0 is the water uptake at $t = 0$ s, w_{eq} is the equilibrium uptake in the test conditions, R_p is the particle radius (assumed to be half of the grain size, under the approximation of spherical beads), F_0 is a shape factor equal to 15 in the case of spheres, and D is the diffusivity. The second one is modified LDF (LDFDw)[19]:

$$\frac{w(t) - w_0}{w_{eq} - w_0} = \frac{e^{\frac{F_0 \cdot (a + b\cdot w_{eq})}{R_p^2}t} - 1}{e^{\frac{F_0 \cdot (a + b\cdot w_{eq})}{R_p^2}t} + b\cdot\frac{w_{eq} - w_0}{a + b\cdot w_0}} \quad \text{(Equation 5)}$$

where t, w_0, w_{eq}, R_p, F_0 have the same meaning as in Equation (4). The constant diffusivity D is replaced by a linear function of water uptake: $D(w) = a + b\cdot w$, with a and b being the model's main parameters. The LDFDw model is a generalization of the LDF model (when $b = 0$, the two models coincide), and takes into account that, when a large range of uptake is considered, the diffusivity cannot be assumed constant. The two models have been used to estimate the vapor transport diffusivity through a least squares fitting procedure,[60] starting from the experimental data available on the material. Starting from the diffusivity and the equilibrium values known from the isotherms, we simulated repetitive cycles of adsorption followed by desorption (details in Note S12, Figure S18). This allowed us to estimate the theoretical SDWP expected under various test conditions and trace the red curve in Figure 4B.

Experimental campaign in the desalination unit

Each experimental test consists of a repetition of 3–6 consecutive cycles at fixed conditions. Each cycle consists of three sequential phases.

- Adsorption phase: valve V2 is opened and valve V3 is closed, so that the feedwater in the EV tank evaporates, fills the EV tank and adsorber chamber, and it is adsorbed by the sorbent material; the exchanger is cooled down by the external circuit and the EV tank water is heated up by the other external circuit.
- Desorption phase: valve V2 is closed and valve V3 is opened; the material is heated up by the external circuit, using the heater H7, and water condenses on the adsorber internal walls and falls by gravity into the CD pipe.
- Pre-cooling phase: valves V2 and V3 are closed; the material is cooled down again in preparation for the adsorption phase of the successive cycle, for 15–17 min, depending on the desorption temperature; during this time interval, the CD pipe is emptied of the condensed water, and vacuum is made again in this portion of the circuit.

The parameters that can be controlled during a test are: T_{EV} (EV tank temperature during adsorption, with control feedback sensor T5), T_{Ads} (adsorber temperature during adsorption, with control feedback sensor T1), T_{Des} (adsorber temperature during desorption, with control feedback sensor T1), t_{Ads} (adsorption time, i.e., the duration of the adsorption phase), t_{Des} (desorption time, i.e., the duration of the desorption phase), and t_{Cool} (pre-cooling time, i.e., the duration of the pre-cooling phase).

Before starting the actual experimental campaign, the material had been subjected to 50 cycles under vacuum within the machine, adsorbing and desorbing vapor in conditions analogous to those of the subsequent experimental campaign. This allowed the material to stabilize and lose any residual water from production, as well as to characterize the material aging over the cycles; after 20, 30, and 40 cycles, the machine was opened and a small sample of material was removed and stored for successive testing (Figure 2B) to check how the material performance changed.

After the preliminary cycles, a full experimental campaign (tests 1 – 9 in Table 1) has been performed. In the campaign,

Table 1. Tests conducted in the desalination unit

Test	1	2	3	4	5	6	7	8	9
Material	CA	CA	CA	CA	CA	CA	SG	SG	SG
T_{Des} (°C)	60	45	75	60	60	60	60	45	75
t_{Des} (min)	120	120	120	60	45	30	120	120	120

Material, desorption temperature, and desorption time are specified. CA, calcium alginate and SG, mesoporous silica gel.

T_{Ads} and T_{EV} were kept constant, both equal to 30°C; the adsorption time t_{Ads} was kept constant and equal to 30 min; t_{Cool} was chosen always equal to 15 min (17 min for the tests at 75°C). On the other hand, the desorption temperature T_{Des} and time t_{Des} as well as the sorbent material were changed in a one-factor-at-a-time approach. This does not allow a complete characterization of the machine, but it helps in understanding the influence of the parameters taken separately.

A preliminary start-up procedure is carried out every time the material is replaced (more details in Note S13, Figure S19). Then, for each test, the normal experimental procedure is described here.

(1) The water level in the EV tank is restored (approximately 4.5 L at the beginning of all tests).
(2) The vacuum pump is powered 10 min to remove any residual air in the EV tank before starting the test.
(3) The testing parameters are adjusted according to Table 1.
(4) The external circuits are powered and the temperatures of both the EV tank and adsorber are brought to 30°C, in preparation for the adsorption phase of the first cycle.
(5) The first cycle starts and phases 1 to 3 run in sequence.
(6) During phase 3, the condensed water is collected from the CD pipe and weighed on a KERN PCB scale (accuracy of 0.1 g).
(7) The vacuum pump is connected to the CD pipe (valve VB) and it is powered for 1 min to remove the air entering the CD pipe during the water collection and 1 further min with V3 open to remove any residual vapor in the chamber (see also Note S14).
(8) Points 5 to 7 repeat for the successive cycles of the day.

All the tests started in the morning around 9:00 a.m. central European time and have taken place during the month of March 2025, trying to minimize the influence of seasonal variations in the room temperature.

The main aim of this research was to compare the thermal cycles and the mass transport of water, rather than the desalination performance (i.e., the solute rejection rate); thus, in most of the tests run in the machine, we used distilled water in the EV tank. Replacing distilled water with salty water might change the water fugacity; therefore, a detailed and comprehensive investigation using salty water is left to future campaigns. For the limited scope of this work, in order to preliminarily test the ability of hydrogel to work with a salty solution, few cycles using salty water were performed after the main experimental campaign and a preliminary analysis has been conducted on the water samples, including estimations of conductivity, solid content, pH, total organic carbon (TOC), and copper (Cu) content (see also Note S6).

Starting from the test results, we evaluated two key performance indicators (KPIs). The first one is SDWP, a KPI indicating the amount of condensed water achievable in 24 h of continuous operation and defined as follows:

$$SDWP = \frac{V_w}{m_{dry}} \cdot \frac{1}{t_{cycle}} \quad \text{(Equation 6)}$$

where V_w is the volume of condensed water produced in a cycle, m_{dry} is the amount of dry sorbent material, t_{cycle} is the duration of the cycle (including adsorption, desorption, and pre-cooling). The used units are $[V_w] = m^3$, $[m_{dry}] = ton$, $[t_{cycle}] = day$, from which: $[SDWP] = m^3/day/ton$.

The second indicator is STEC, a KPI indicating the amount of positive thermal energy used to condensate one liter of water and defined as follows:

$$STEC = \frac{E_{hot}}{V_w} \quad \text{(Equation 7)}$$

where E_{hot} is the thermal energy used during desorption in a test and V_w is the volume of water condensed in the same test. If V_w is evaluated in L and E_{hot} in kWh, then $[STEC] = kWh/L$. The KPIs defined above are then compared with results from the literature.

Further details on the choice of the best-fitting equilibrium model are provided in Note S15 (Figure S20). The experimental dependence of CaAlg beads' volume on RH is discussed in Note S16 (Figure S21). A theoretical discussion on the dependence of SDWP on the CaAlg beads' diameter is provided in Note S17 (Figure S22).

RESOURCE AVAILABILITY

Lead contact

Requests for further information and resources should be directed to the lead contact, Dr. Eliodoro Chiavazzo (eliodoro.chiavazzo@polito.it).

Materials availability

This study did not generate new, unique reagents.

Data and code availability

- Material data on water vapor-calcium alginate equilibrium adsoprtion isotherms have been deposited at Zenodo and are publicly available as of the date of publication at https://doi.org/10.5281/zenodo.18219709.
- This paper does not report original code.
- Any additional information required to reanalyze the data reported in this paper is available from the lead contact upon request.

ACKNOWLEDGMENTS

This study was carried out in the framework of a specific regional call for proposals (Apprendistato di Alta Formazione e Ricerca – Avviso Pubblico 2022–2024 per l'individuazione e la gestione dell'offerta formativa pubblica approvato con Determinazione 114 del 3/3/2022 e s.m.i.) and within the WADERE project, funded by the Ministero dell'Università e della Ricerca – within the PRIN 2022 program (D.D.104 - 02/02/2022). This manuscript reflects only the authors' views and opinions, and the Ministry cannot be considered responsible for them. The authors are grateful to Clean Water Center (Politecnico di Torino) for funding. We are grateful to Walter Mittelbach (from Sorption Technologies GmbH) for the fruitful technical discussions. We are also grateful to Gabriele Penello, Abhijeet Khot, and Gabriel Yarce (from Sorption Technologies GmbH) for their help with enhancing the design of the desalination unit. The authors gratefully acknowledge the support of Fabrizio Bianco, Lorenzo

Craveri, and Prof. Alberto Tiraferri (DIATI, Politecnico di Torino) for assistance with total organic carbon (TOC) and copper (Cu) analyses.

AUTHOR CONTRIBUTIONS

M.C. and E.C. conceived the experiments and supervised the work. M.C. performed the experiments. M.C., E.C., V.G., and M.F. analyzed the data, interpreted the results, and wrote and reviewed the paper. E.C., V.G., and M.F. contributed materials and analysis tools.

DECLARATION OF INTERESTS

The authors declare no competing interests.

SUPPLEMENTAL INFORMATION

Supplemental information can be found online at https://doi.org/10.1016/j.xcrp.2026.103139.

Received: August 25, 2025
Revised: November 19, 2025
Accepted: January 19, 2026

REFERENCES

1. Mekonnen, M.M., and Hoekstra, A.Y. (2016). Four billion people facing severe water scarcity. Sci. Adv. *2*, e1500323.
2. Skuse, C., Gallego-Schmid, A., Azapagic, A., and Gorgojo, P. (2021). Can emerging membrane-based desalination technologies replace reverse osmosis? Desalination *500*, 114844.
3. Shatat, M., Worall, M., and Riffat, S. (2013). Opportunities for solar water desalination worldwide: Review. Sustain. Cities Soc. *9*, 67–80.
4. Abanyie, S.K., Apea, O.B., Abagale, S.A., Amuah, E.E.Y., and Sunkari, E.D. (2023). Sources and factors influencing groundwater quality and associated health implications: A review. Emerging Contam. *9*, 100207.
5. Chandrashekara, M., and Yadav, A. (2016). Water desalination system using solar heat: A review. Renew. Sustain. Energy Rev. *67*, 1208–1330.
6. Aladwani, S.H., Al-Obaidi, M.A., and Mujtaba, I.M. (2021). Performance of reverse osmosis based desalination process using spiral wound membrane: Sensitivity study of operating parameters under variable seawater conditions. Cleaner Engineering and Technology *5*, 100284.
7. Ashafan, H., Sultan, M., Miyazaki, T., Saha, B.B., Askalany, A.A., Shahzad, M.W., and Worek, W. (2022). Recent development in adsorption desalination: A state of the art review. Appl. Energy *328*, 120101.
8. Abu Dhabi Environment Agency, Energy efficient desalination, presented at International Water Summit, 2018 (unpublished).
9. Chiavazzo, E., Morciano, M., Viglino, F., Fasano, M., and Asinari, P. (2018). Passive solar high-yield seawater desalination by modular and low-cost distillation. Nat. Sustain. *1*, 763–772.
10. Morciano, M., Fasano, M., Boriskina, S.V., Chiavazzo, E., and Asinari, P. (2020). Solar passive distiller with high productivity and Marangoni effect-driven salt rejection. Energy Environ. Sci. *13*, 3646–3655.
11. Morciano, M., Fasano, M., Bergamasco, L., Albiero, A., Lo Curzio, M., Asinari, P., and Chiavazzo, E. (2020). Sustainable freshwater production using passive membrane distillation and waste heat recovery from portable generator sets. Appl. Energy *258*, 114086.
12. Morciano, M., Fasano, M., Salomov, U., Ventola, L., Chiavazzo, E., and Asinari, P. (2017). Efficient steam generation by inexpensive narrow gap evaporation device for solar applications. Sci. Rep. *7*, 11970.
13. Daßler, I., and Mittelbach, W. (2012). Solar Cooling with Adsorption Chillers. Energy Proc. *30*, 921–929.
14. Frazzica, A., Zhang, Y., Bonanno, A., Palomba, V., and Brancato, V. (2023). Innovative Low-Grade Sorption Desalination Technology for Application on Board of Vessels, Presented at ECOS (Las Palmas De Gran Canaria).
15. Lokare, O.R., Ji, P., Wadekar, S., Dutt, G., and Vidic, R.D. (2019). Concentration polarization in membrane distillation: I. Development of a laser-based spectrophotometric method for in-situ characterization. J. Memb. Sci. *581*, 462–471.
16. Ristic, A., Logar, N.Z., Henninger, S.K., and Kaucic, V. (2012). The Performance of Small-Pore Microporous Aluminophosphates in Low-Temperature Solar Energy Storage: The Structure-Property Relationship. Adv. Funct. Mater. *22*, 1952–1957.
17. Ristic, A., and Henninger, S.K. (2014). Sorption Composite Materials for Solar Thermal Energy Storage. Energy Proc. *48*, 977–981.
18. Krajnc, A., Varlec, J., Mazaj, M., Ristic, A., Logar, N.Z., and Mali, G. (2017). Superior Performance of Microporous Aluminophosphate with LTA Topology in Solar-Energy Storage and Heat Reallocation. Adv. Energy Mater. *7*, 1601815.
19. Gentile, V., Calò, M., Bozlar, M., Simonetti, M., and Meggers, F. (2024). Water vapor mass transfer in alginate–graphite bio-based hydrogel for atmospheric water harvesting. Int. J. Heat Mass Tran. *219*, 124794.
20. Khan, M.A., Thu, K., and Mitra, S. (2024). Experimental evaluation of Adsorption Heat for Water vapour/Silica gel pair for chiller application. Appl. Therm. Eng. *249*, 123289.
21. Tralidis, G.A., Dias, D., Martins, A., Vasilaki, V., Ribeiro, J.M., and Katsou, E. (2025). Assessing the ISO hierarchy validity in circular wastewater treatment life cycle assessments: A Portuguese case study. Resour. Conserv. Recycl. *215*, 108146.
22. Wagle, S.R., Kovacevic, B., Ionescu, C.M., Walker, D., Jones, M., Carey, L., Takechi, R., Mikov, M., Mooranian, A., and Al-Salami, H. (2021). Pharmacological and Biological Study of Microencapsulated Probucol-Secondary Bile Acid in a Diseased Mouse Model. Pharmaceutics *13*, 1223.
23. Nilsson, A.E., Bergman, K., Gomez Barrio, L.P., Cabral, E.M., and Tiwari, B.K. (2022). Life cycle assessment of a seaweed-based biorefinery concept for production of food, materials, and energy. Algal Res. *65*, 102725.
24. Kumar, A. Introduction to Alginate: Biocompatible, Biodegradable, Antimicrobial Nature and Various Applications (Ihana Aguiar Severo and André Bellin Mariano and José Viriato Coelho Vargas, 2024).
25. Pawar, S.N., and Edgar, K.J. (2012). Alginate derivatization: A review of chemistry, properties and applications. Biomaterials *33*, 3279–3305.
26. Sikorski, P., Mo, F., Skjåk-Braek, G., and Stokke, B.T. (2007). Evidence for Egg-Box-Compatible Interactions in Calcium-Alginate Gels from Fiber X-ray Diffraction. Biomacromolecules *8*, 2098–2103.
27. Plazinski, W. (2011). Molecular Basis of Calcium Binding by Polyguluronate Chains. Revising the Egg-Box Model. J. Comput. Chem. *32*, 2988–2995.
28. ISO, *9277*:2022 - Determination of the specific surface area of solids by gas adsorption - BET method (2022).
29. Blahovec, J., and Yanniotis, S. (2008). GAB Generalized Equation for Sorption Phenomena. Food Bioproc. Tech. *1*, 82–90.
30. Kim, H., Cho, H.J., Narayanan, S., Yang, S., Furukawa, H., Schiffres, S., Li, X., Zhang, Y.B., Jiang, J., Yaghi, O.M., and Wang, E.N. (2016). Characterization of Adsorption Enthalpy of Novel Water-Stable Zeolites and Metal-Organic-Frameworks. Sci. Rep. *6*, 19097.
31. Timmermann, E.O. (2003). Multilayer sorption parameters: BET or GAB values? Colloids Surf. A Physicochem. Eng. Asp. *220*, 235–260.
32. Li, L., Fang, Y., Vreeker, R., Appelqvist, I., and Mendes, E. (2007). Reexamining the Egg-Box Model in Calcium¨ Alginate Gels with X-ray Diffraction. Biomacromolecules *8*, 464–468.
33. Gentile, V., Bozlar, M., Calò, M., Simonetti, M., and Meggers, F. (2024). Alginate Biopolymeric Coated Heat Exchanger for Atmospheric Water Harvesting. ACS ES&T Water *4*.

34. Mignon, A., Snoeck, D., D'Halluin, K., Balcaen, L., Vanhaecke, F., Dubruel, P., Van Vlierberghe, S., and De Belie, N. (2016). Alginate biopolymers: Counteracting the impact of superabsorbent polymers on mortar strength. Constr. Build. Mater. *110*, 169–174.

35. Safronov, A.P., Kurilova, N.M., Adamova, L.V., Shklyar, T.F., Blyakhman, F.A., and Zubarev, A.Y. (2023). Hydrogels Based on Polyacrylamide and Calcium Alginate: Thermodynamic Compatibility of Interpenetrating Networks, Mechanical, and Electrical Properties. Biomimetics *8*, 279.

36. Mittal, H., Al Alili, A., and Alhassan, S.M. (2020). Adsorption isotherm and kinetics of water vapors on novel superporous hydrogel composites. Microporous Mesoporous Mater. *299*, 110106.

37. Palomba, V., Frazzica, A., Brancato, V., Bonanno, A., Zhang, Y., Calò, M., Penello, G., Yarce, G., and Mittelbach, W. (2025). Experimental proof of a thermal system for cooling and storage applications employing cacl2/silica gel composite adsorbent. Energy Convers. Manag. *341*, 120072.

38. Mohammed, R.H., Rupam, T.H., Nunez, R., Spitzenberger, J., Mohammadian, S.K., Lee, J., Saha, B.B., and Ma, H. (2023). Comparative analysis of four metal-organic frameworks for adsorption desalination. Colloids Surf. A Physicochem. Eng. Asp. *673*, 131750.

39. Bo, H., Mai Sheng, N., and Anutosh, C. (2025). Optimizing metal-organic frameworks for adsorption-based atmospheric water harvesting: A systematic evaluation of pristine and modified MOFs for enhanced performance in diverse climates. Chem. Eng. J. *521*, 166607.

40. Rodgers, R.C., and Hill, G.E. (1978). Equations for vapour pressure versus temperature: derivation and use of the Antoine equation on a hand-held programmable calculator. Br. J. Anaesth. *50*, 415–424.

41. Wu, J.W., Biggs, M.J., and Hu, E.J. (2014). Dynamic model for the optimisation of adsorption-based desalination processes. Appl. Therm. Eng. *66*, 464–473.

42. World Health Organization (2022). Guidelines for Drinking-Water Quality, Fourth Edition (World Health Organization).

43. Rusydi, A.F. (2018). Correlation between conductivity and total dissolved solid in various type of water: A review. IOP Conf. Ser. Earth Environ. Sci. *118*, 012019.

44. Ali, E.S., Askalany, A.A., Harby, K., Diab, M.R., Hussein, B.R., and Alsaman, A.S. (2021). Experimental adsorption water desalination system utilizing activated clay for low grade heat source applications. J. Energy Storage *43*, 103219.

45. Xiaolin, W., Hui Tong, C., and Kim Choon, N. (2005). Experimental investigation of silica gel–water adsorption chillers with and without a passive heat recovery scheme. Int. J. Refrig. *28*, 756–765.

46. Thu, K., Ng, K.C., Saha, B.B., Chakraborty, A., and Koyama, S. (2009). Operational strategy of adsorption desalination systems. Int. J. Heat Mass Tran. *52*, 1811–1816.

47. Ng, K.C., Thu, K., Chakraborty, A., Saha, B.B., and Chun, W.G. (2009). Solar-assisted dual-effect adsorption cycle for the production of cooling effect and potable water. Int. J. Low Carbon Technol. *4*, 61–67.

48. Alsaman, A.S., Askalany, A.A., Harby, K., and Ahmed, M.S. (2017). Performance evaluation of a solar-driven adsorption desalination-cooling system. Energy *128*, 196–207.

49. Ghazy, M., Askalany, A.A., Ibrahim, E., Mohamed, A., Ali, E.S., and AL-Dadah, R. (2022). Solar powered adsorption desalination system employing CPO-27(Ni). J. Energy Storage *53*, 105174.

50. Elsayed, E., AL-Dadah, R., Mahmoud, S., Anderson, P., and Elsayed, A. (2020). Experimental testing of aluminium fumarate MOF for adsorption desalination. Desalination *475*, 114170.

51. Olkis, C., Brandani, S., and Santori, G. (2019). Design and experimental study of a small scale adsorption desalinator. Appl. Energy *253*, 113584.

52. Olkis, C., Brandani, S., and Santori, G. (2019). A small-scale adsorption desalinator. Energy Proc. *158*, 1425–1430.

53. Ibrahim, A., Elsheniti, M.B., AL-Dadah, R., Mahmoud, S., and Solmaz, I. (2022). Numerical and experimental investigation of multiple heat exchanger modules in cooling and desalination adsorption system using metal organic framework. Energy Convers. Manag. *251*, 114924.

54. Luberti, M., Gowans, R., Finn, P., and Santori, G. (2022). An estimate of the ultralow waste heat available in the European Union. Energy *238*, 121967.

55. Mytton, D. (2021). Data centre water consumption. npj Clean Water *4*, 11.

56. Alissa, H., Nick, T., Raniwala, A., Arribas Herranz, A., Frost, K., Manousakis, I., Lio, K., Warrier, B., Oruganti, V., DiCaprio, T.J., et al. (2025). Using life cycle assessment to drive innovation for sustainable cool clouds. Nature *641*, 331–338.

57. Skjåk-Bræk, G., Grasdalen, H., and Smidsrød, O. (1989). Inhomogeneous Polysaccharide Ionic Gels. Carbohydr. Polym. *10*, 31–54.

58. Crank, J. (1975). The Mathematics of Diffusion (Oxford University Press).

59. Ruthven, D.M. (1984). Principles of Adsorption and Adsorption Processes (Wiley).

60. Bickel, P.J., and Doksum, K.A. (2015). Mathematical Statistics (CRC Press).

Cell Reports Physical Science, Volume *7*

Supplemental information

Calcium alginate hydrogel for high-yield adsorption-based desalination driven by ultralow-grade heat

Matteo Calò, Vincenzo Gentile, Matteo Fasano, and Eliodoro Chiavazzo

Note S1 – Comparison with literature

In Table s1 we provide the data considered for Fig. 4c in the main text. Note that Specific Thermal Energy Consumption (STEC) is not always available in literature. When not explicitly reported, it was estimated starting from the Performance Ratio (PR), or starting from the Specific Cooling Power (SCP) and the thermal Coefficient Of Performance (COP), as follows:

$$STEC \sim \frac{H_{liq}}{3600 \cdot PR} \qquad \text{or} \qquad STEC \sim \frac{SCP \cdot 24}{SDWP \cdot COP \cdot 1000}$$

where H_{liq} is the evaporation heat of water at the considered temperature (2430 kJ/kg at 30°C), the Specific Daily Water Production $SDWP$ is expressed in $m^3/day/ton$, and the numerical constants are introduced to have the final $STEC$ output expressed in kWh/L.

Plant	*Sorbent*	*Amount of material (kg)*	*Desorption temperature (°C)*	*SDWP (m^3/day/ton)*	*STEC (kWh/L)*	
This research	CaAlg	0.386	45	2.22	1.55	-
This research	CaAlg	0.386	60	6.04	0.97	-
This research	CaAlg	0.386	75	4.51	1.41	-
[S1], two-beds	Silica-gel	72	75	7.52	1.05	Estimated starting from PR
[S1], four-beds	Silica-gel	144	85	10	1.11	Estimated starting from PR
[S2]	Silica-gel	72	65	5.8	0.99	Estimated starting from PR
[S3]	Silica-gel	13.5	76	3.7	1.46	Estimated starting from SCP
[S3]	Silica-gel	13.5	89	3.92	1.56	Estimated starting from SCP
[S4], mode1	MOF CPO-27(Ni)	1.8	95	4.8	-	Not available
[S 4], mode2	MOF CPO-27(Ni)	1.8	95	10.2	-	Not available
[S 4], mode1	MOF CPO-27(Ni)	1.8	80	1.9	-	Not available
[S 4], mode2	MOF CPO-27(Ni)	1.8	80	5.2	-	Not available
[S 5]	Aluminium fumarate	1.5	70	8.23	-	Not available
[S 5]	Aluminium fumarate	1.5	90	8.48	-	Not available
[S 6]	Silica-gel	0.2	80	7.7	1.08	Estimated starting from PR
[S 7]	Aluminium fumarate	23.2	85	8.6	1.26	Estimated starting from SCP
[S 7]	Aluminium fumarate	23.2	60	7.2	1.28	Estimated starting from SCP

Table s1: Comparison of this research's KPIs with plants from literature.

In table s2 we report a comparison of some of the material properties (equilibrium water uptake at 70%, enthalpy of adsorption) with values from literature.

Material	*Equilibrium water uptake at T=30°C, RH=70% (g/g)*	*Hads (kJ/kg)*
CaAlg (this research)	1.28	2600
RD 8-14 Silica-gel,[S8]	0.36	2690
CaCl2/Silica-gel, [S9]	0.75	2530÷2633
Zeo-K-X, [S10]	0.11	15600
Zeo-Na-X, [S10]	0.18	6670
Zeo-Mg-X, [S10]	0.24	2030
Zeo-Ca-X, [S10]	0.2	1610
CAU-10 H, [S11]	0.31	2762

Table s2: Equilibrium water uptakes at RH=70% and enthalpies of adsorption for CaAlg and materials from literature.

Note S2 – CaAlg appearance

The CaAlg beads have a grain size of approximately 1.5 mm and a CaAlg density of approximately $\rho_{CaAlg} \sim 2000 \pm 400\ kg/m^3$. For the sake of simplicity, the CaAlg beads are approximated as spheres when needed in the calculations, and the grain size is used as sphere diameter (the same approximation is done with silica-gel beads).

By cycling in the machine, the material appearance has slightly changed from the 'as produced' beads:

- the colour has become browner (Fig. s1), probably because of some caramelization happened when the material was brought up to 75°C in the desalination unit;
- the diameter of the particles has slightly reduced, from 1.57 mm (average on measurements on 10 beads, with standard deviation of 0.12 mm) to 1.43 mm (average on 10 beads, with standard deviation of 0.10 mm). The measurements have been taken used a micrometre with accuracy of 0.001 mm. Also, the same beads were weighted: by knowing mass and diameter, the density of $\rho_{CaAlg} \sim 2000 \pm 400\ kg/m^3$ was estimated.

Figure s1: Beads of CaAlg 'as produced' (left) and 'after 40 cycles' (right).

Note S3 – Uncertainties in the evaluation of thermal power

The uncertainties in the temperature measurements translate in high uncertainties in the energy calculations. Thermal power along time is evaluated as follows:

$$P = \rho \cdot Q \cdot c_p \cdot (T_1 - T_2)$$

being $\rho = 1000\ kg/m^3$ the density of the water in the external circuit, $c_p = 4186\ J/(kg \cdot K)$ its specific heat and $Q = 3.4\ L/min$ the volumetric flowrate in the external circuit. In the plot in the main text, the original data has been smoothed with a moving average.

Even by assuming ρ and c_p to be exact, and taking into account only the uncertainty on Q (± 0.2 L/min) and temperatures T_1 and T_2 ($\pm 0.27\ °C$ for class-A PT1000s at 60°C), here is how the uncertainties propagate to P:

$$\left(\frac{\Delta P}{P}\right) = \sqrt{\left(\frac{0.2\ L/min}{Q}\right)^2 + \left[\frac{\sqrt{(0.27°C)^2 + (0.27°C)^2}}{T_1 - T_2}\right]^2}$$

For instance, in the case of a representative cycle from the first test of the campaign (test #1), 20 minutes after the desorption phase starts, it was measured: $T_1 = 59.5\ °C$, $T_2 = 58.7\ °C$, $Q = 3.4\ L/min$, from which: $P = 189\ W \pm 91\ W$. A relative uncertainty of 48% (which drops down to 38% during adsorption, due the lower uncertainty of $\pm 0.21\ °C$ at 30°C for class-A PT1000s) makes the evaluated power unreliable for quantitative considerations.

The same high uncertainty propagates to the calculation of the Specific Thermal Energy Consumption (STEC):

$$STEC = \frac{E_{hot}}{V_w} = \frac{\bar{P} \cdot t_{cycle}}{V_w}$$

where $\bar{P}$ is the "hot" power during the test averaged over time, V_w is the volume of condensed water and t_{cycle} is the total cycle time (adsorption plus desorption and pre-cooling phases times). Assuming negligible uncertainty on V_w (the scale used to measure the collected water has an accuracy of 0.1 g, while the volume V_w is in the order of $10^3 \div 10^4\ mL$), and since t_{cycle} is set and exact by definition, the relative uncertainty of STEC coincides with the one of $\bar{P}$.

If, for simplicity, we assume $\frac{\Delta \bar{P}}{\bar{P}} \approx 48\%$ as above, then we have $\frac{\Delta STEC}{STEC} \approx 48\%$.

Note S4 – Results of the experimental campaign

We report the results of the experimental campaign in Table s3. For all tests, adsorption time and adsorption temperature were kept constant and equal to 30 min and 30 °C, respectively.

Test #		1	2	3	4	5	6	7	8	9
Sorbent material		CaAlg	CaAlg	CaAlg	CaAlg	CaAlg	CaAlg	Silica-gel	Silica-gel	Silica-gel
Desorption temperature (°C)		60	45	75	60	60	60	60	45	75
Desorption time (min)		120	120	120	60	45	30	120	120	120
Specific water condensed per cycle (mL/kg)	*Last cycle*	450.8	254.4	523.3	369.7	377.2	196.6	199.2	242.5	340.8
	Average	448.8	268.0	602.8	407.8	334.4	259.9	252.3	208.6	315.7
	Standard deviation	113	37.4	208	81.0	65.7	64.0	114	70.3	65.8
SDWP (m^3/day/ton)	*Last cycle*	3.93	2.22	4.51	5.07	6.04	3.78	1.74	2.12	2.94
	Average	3.92	2.34	5.20	5.59	5.35	4.99	2.20	1.82	2.72
	Standard deviation	0.99	0.33	1.8	1.1	1.1	1.2	0.99	0.61	0.57
STEC (kWh/L)	Average	1.38	1.55	1.41	1.05	0.97	1.01	1.50	1.37	1.48
	Uncertainty	0.66	0.74	0.68	0.50	0.47	0.48	0.72	0.66	0.71

Table s3: Results of the experimental campaign on CaAlg and mesoporous silica-gel. The testing conditions are reported in the first three rows, followed by KPIs such as specific water production per cycle, per day (SDWP) and the energy cost per Liter (STEC). Volumes (mL, m^3, L) refer to the amount of condensed water; masses (kg, ton) refer to the amount of dry sorbent; energies (kWh) refer to the positive thermal energy entering the system during desorption. Uncertainty for STEC was evaluated in accordance with the estimation discussed in Supplementary 3.

The original data from the tests are reported below.

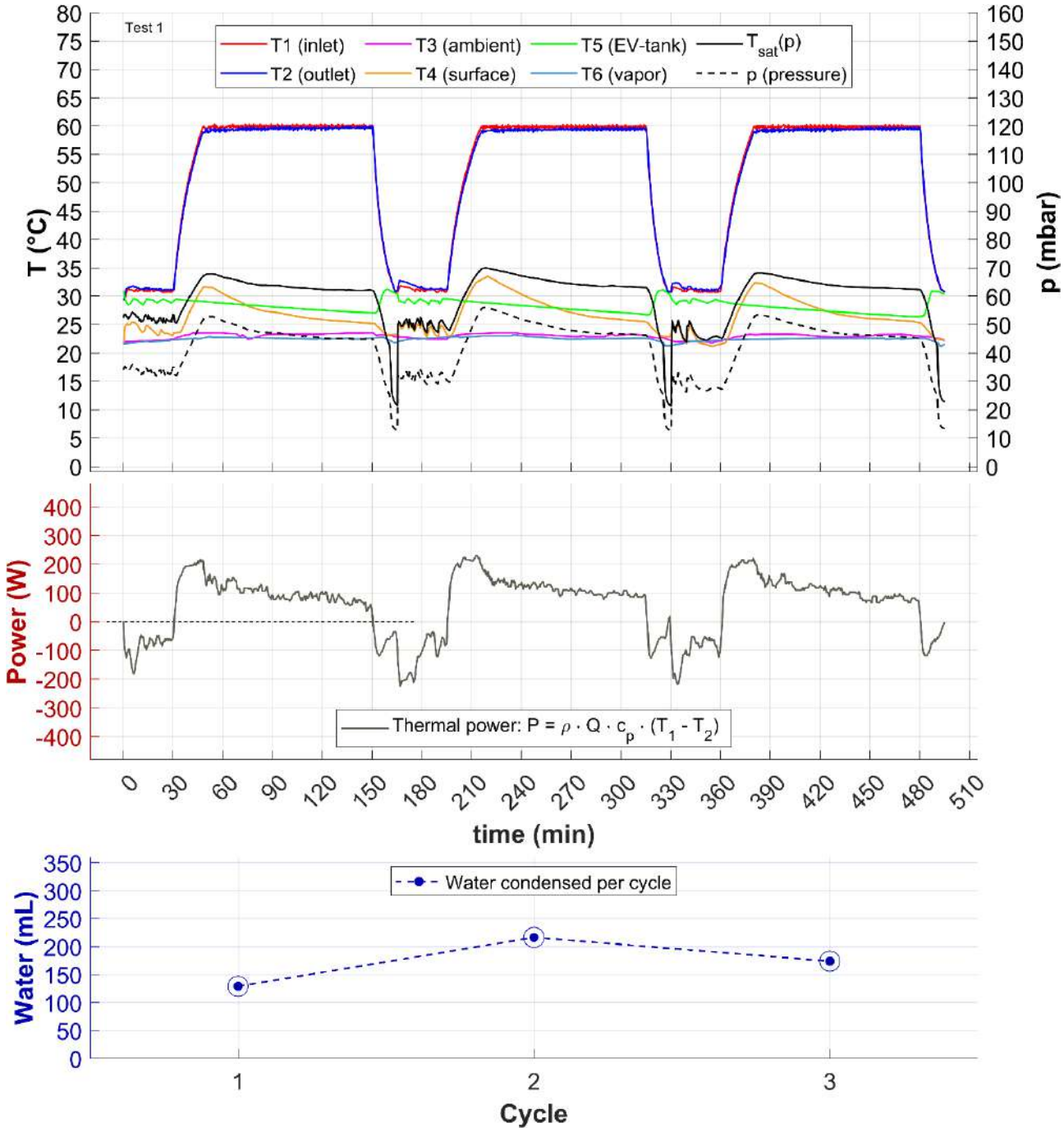

Figure s2: Test 1, material: CaAlg, TADS: 30°C, tADS: 30 min, TDES: 60°C, tDES: 120 min. Sensor T6 (vapor) was not included in the main discussion, given the redundant information it gives with respect to T3. 'p' is vapor pressure in the adsorber.

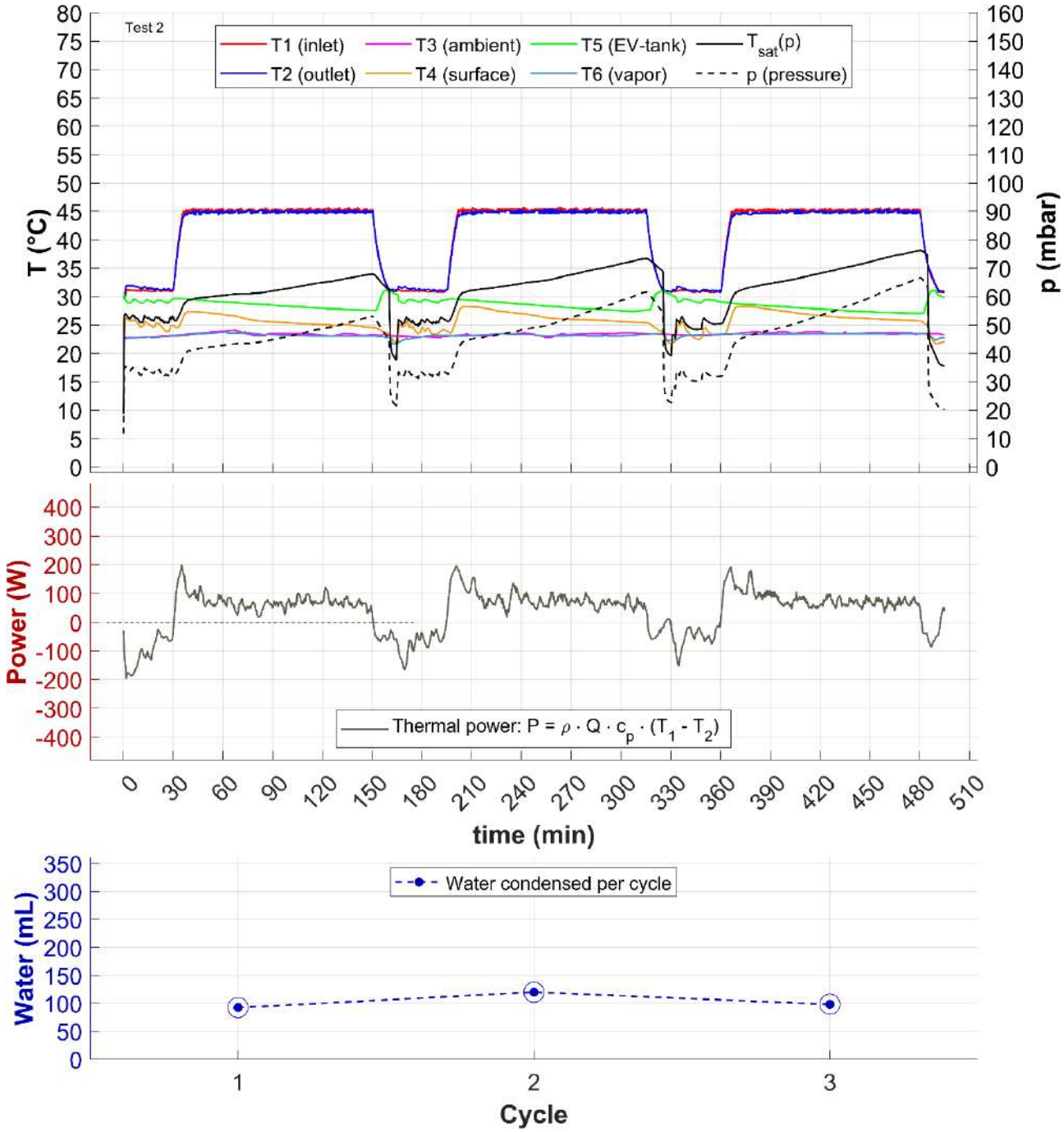

Figure s3: Test 2, material: CaAlg, TADS: 30°C, tADS: 30 min, TDES: 45°C, tDES: 120 min. Sensor T6 (vapor) was not included in the main discussion, given the redundant information it gives with respect to T3. 'p' is vapor pressure in the adsorber.

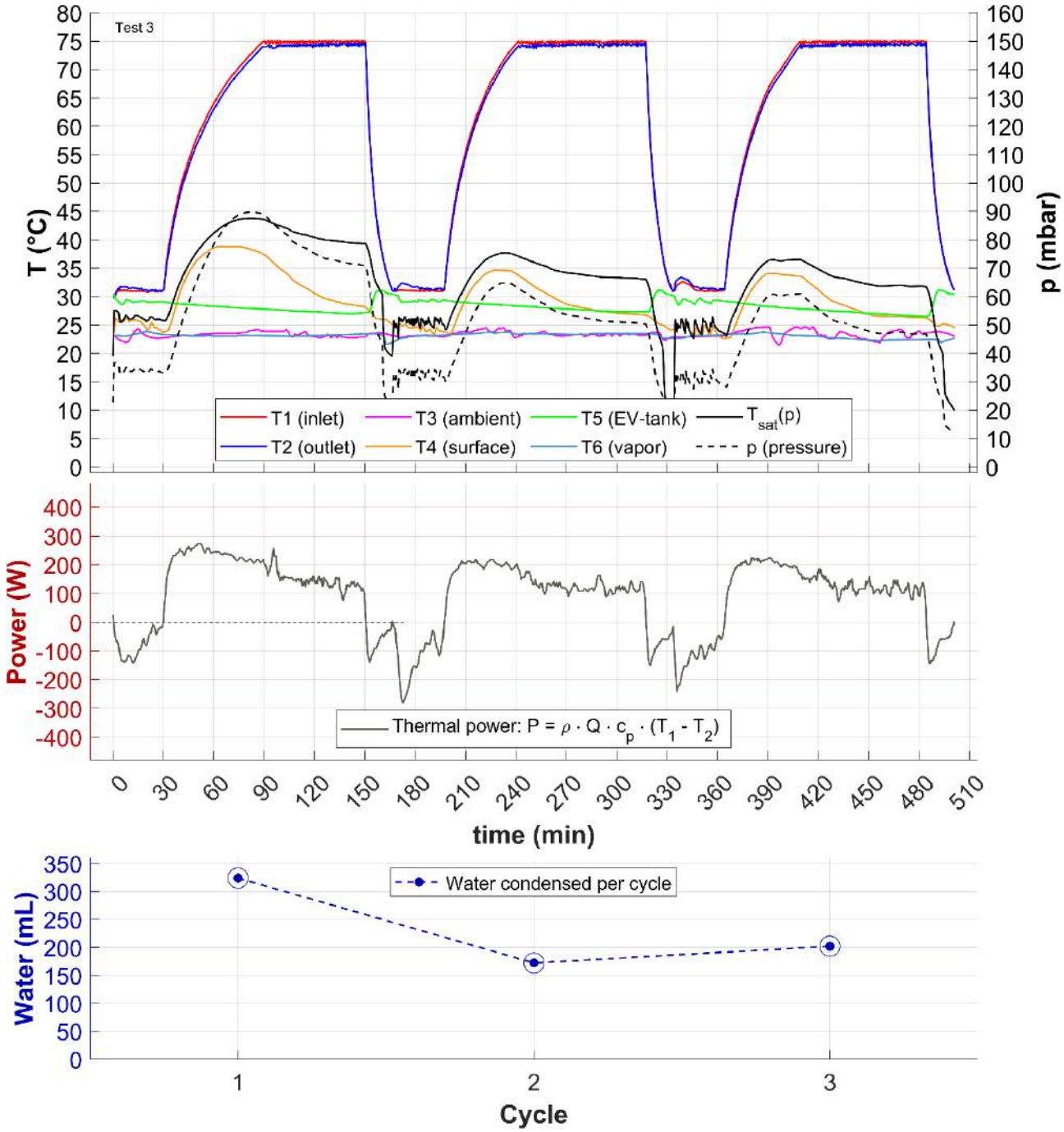

Figure s4: Test 3, material: CaAlg, TADS: 30°C, tADS: 30 min, TDES: 75°C, tDES: 120 min. Sensor T6 (vapor) was not included in the main discussion, given the redundant information it gives with respect to T3. 'p' is vapor pressure in the adsorber.

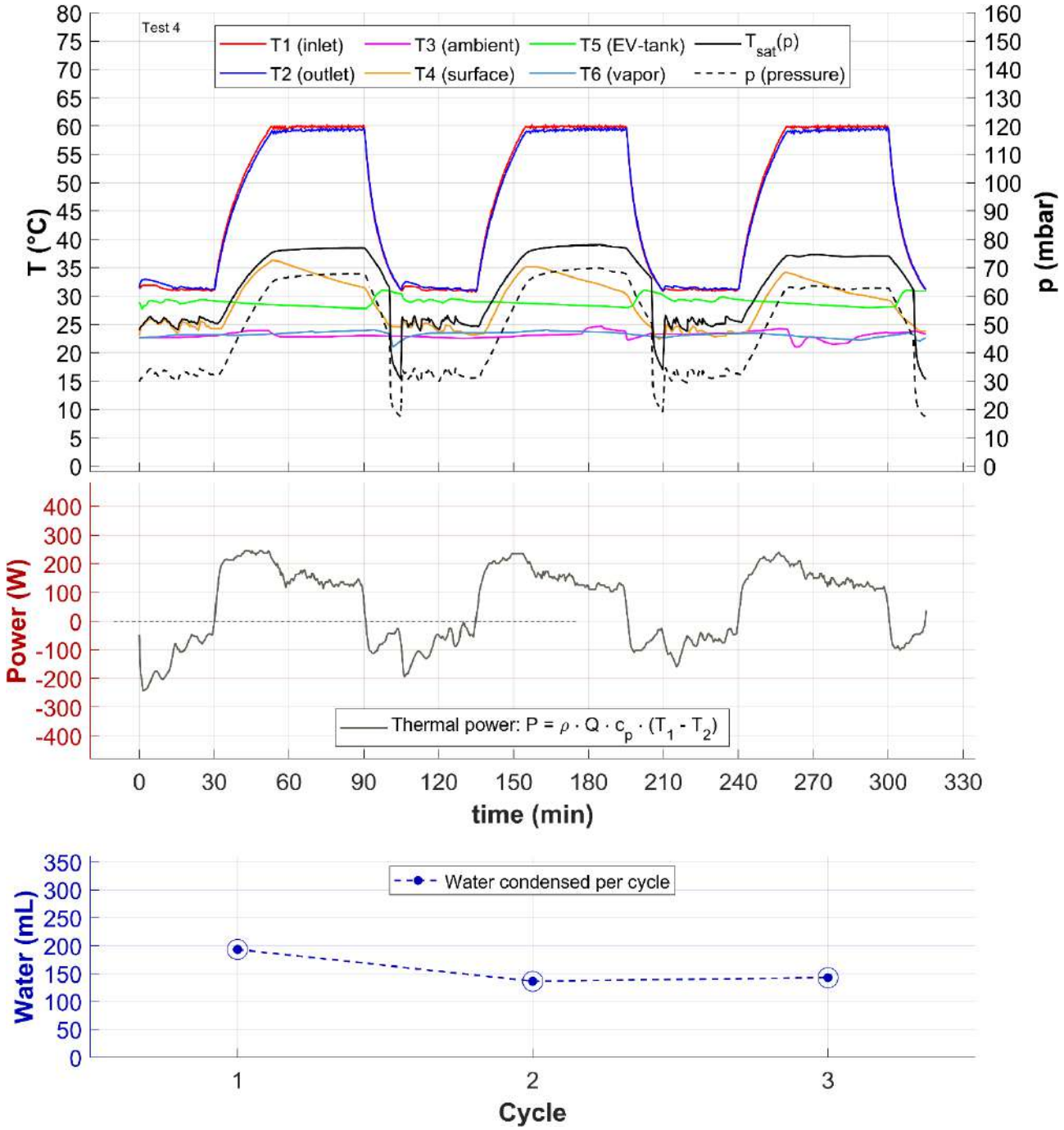

Figure s5: Test 4, material: CaAlg, TADS: 30°C, tADS: 30 min, TDES: 60°C, tDES: 60 min. Sensor T6 (vapor) was not included in the main discussion, given the redundant information it gives with respect to T3. 'p' is vapor pressure in the adsorber.

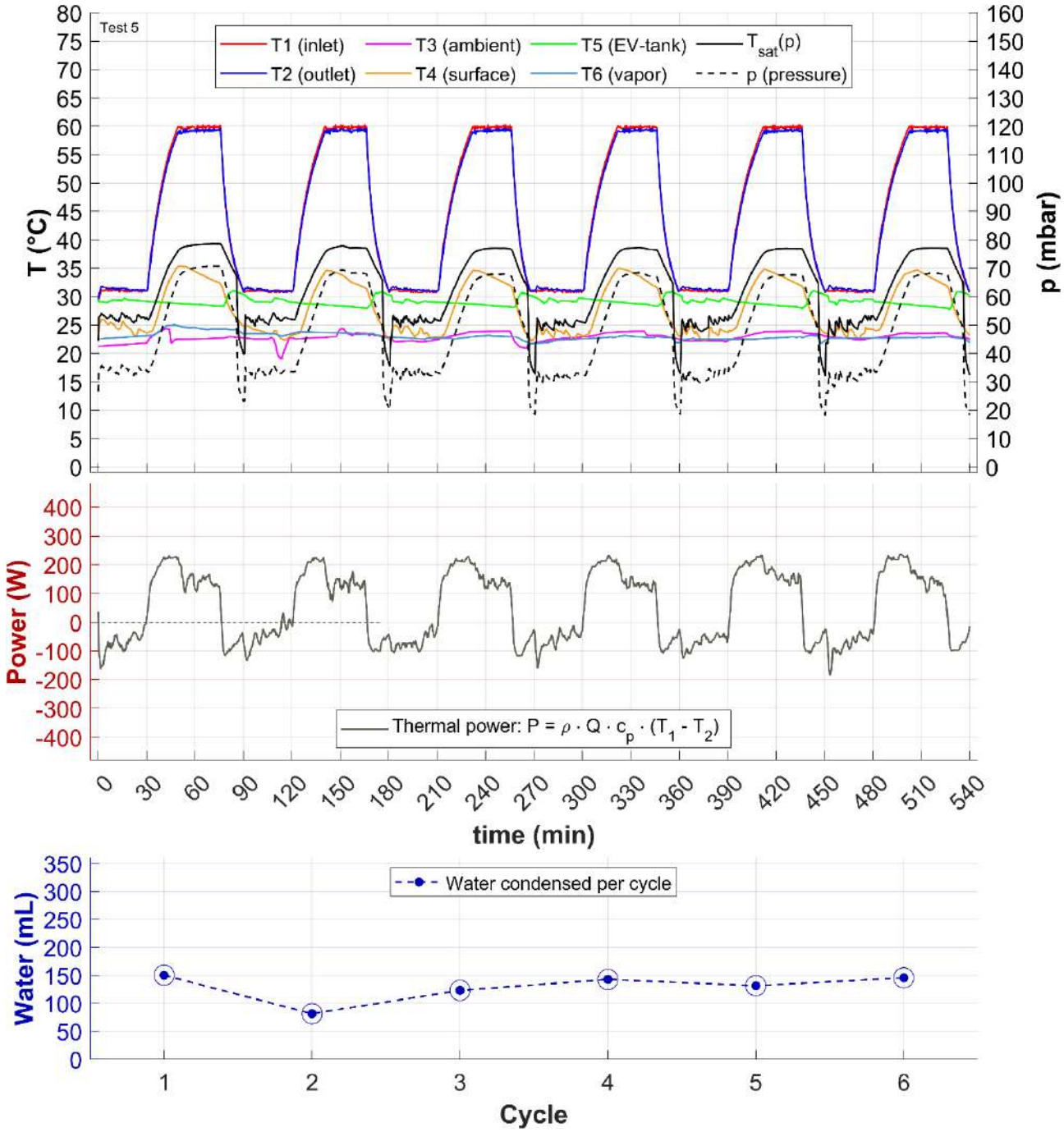

Figure s6: Test 5, material: CaAlg, TADS: 30°C, tADS: 30 min, TDES: 60°C, tDES: 45 min. Six consecutive cycles were carried out. Sensor T6 (vapor) was not included in the main discussion, given the redundant information it gives with respect to T3. 'p' is vapor pressure in the adsorber.

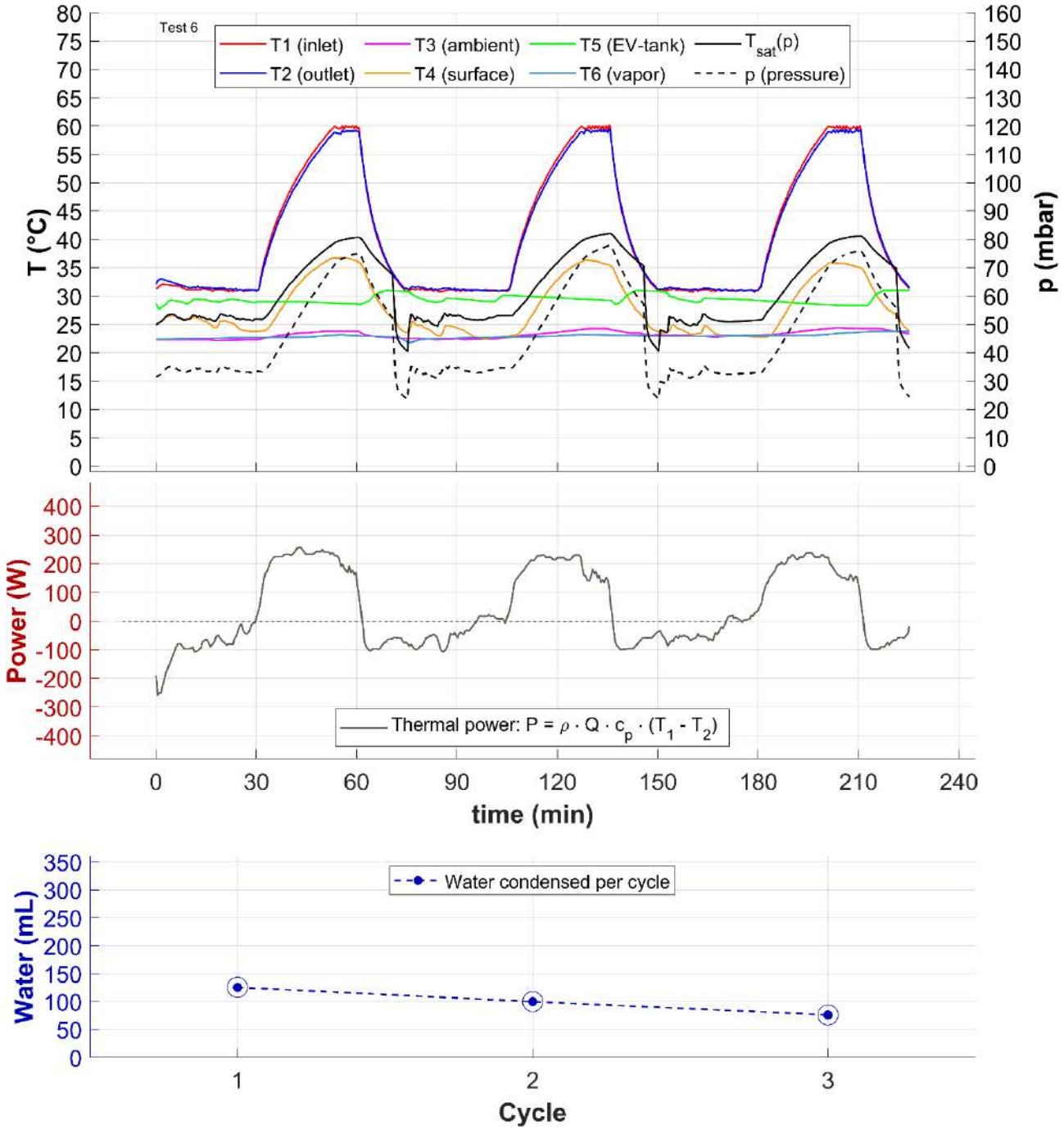

Figure s7: Test 6, material: CaAlg, TADS: 30°C, tADS: 30 min, TDES: 60°C, tDES: 30 min. Sensor T6 (vapor) was not included in the main discussion, given the redundant information it gives with respect to T3. 'p' is vapor pressure in the adsorber.

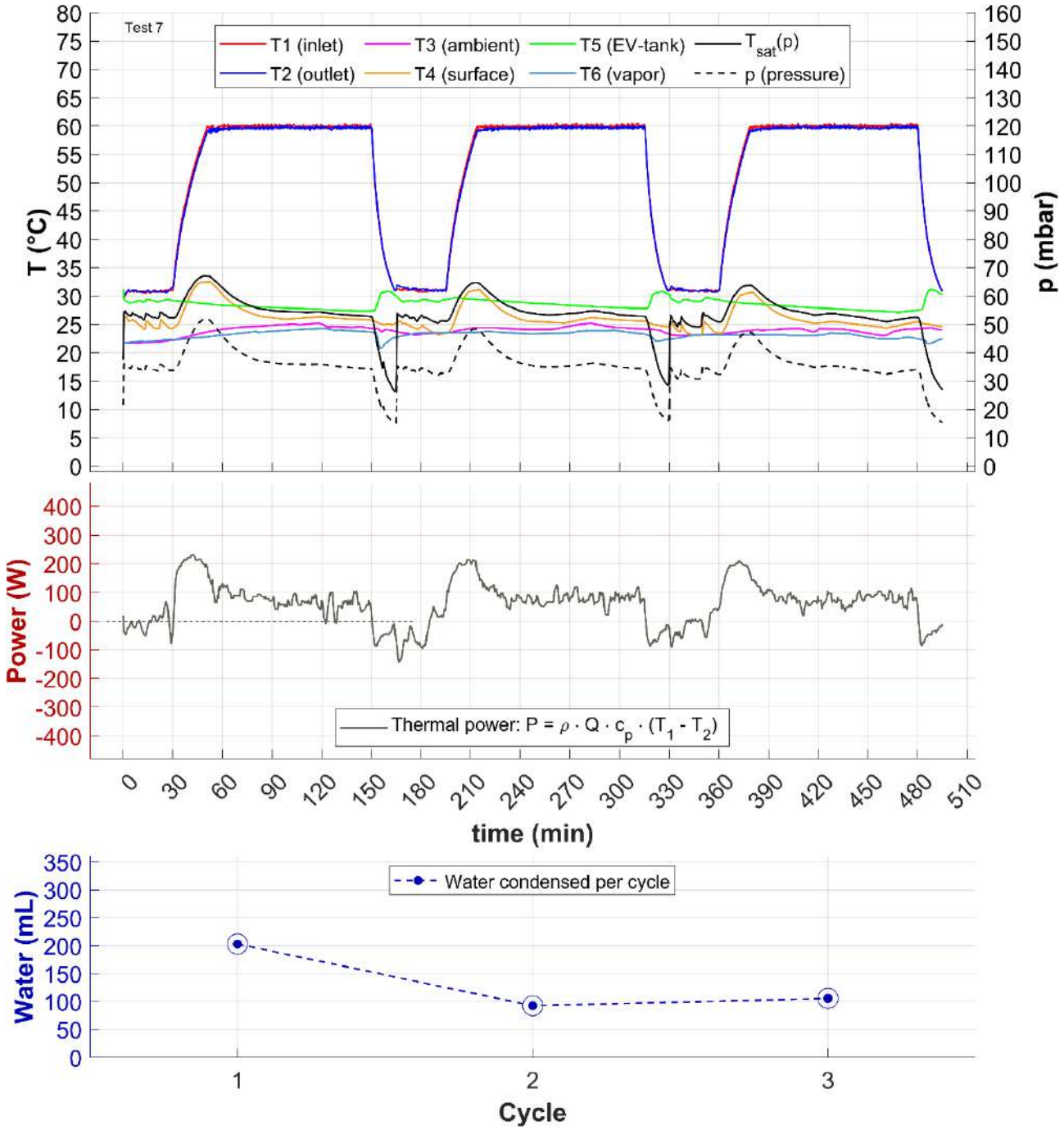

Figure s8: Test7, material: Silica-gel, TADS: 30°C, tADS: 30 min, TDES: 60°C, tDES: 120 min. Sensor T6 (vapor) was not included in the main discussion, given the redundant information it gives with respect to T3. 'p' is vapor pressure in the adsorber.

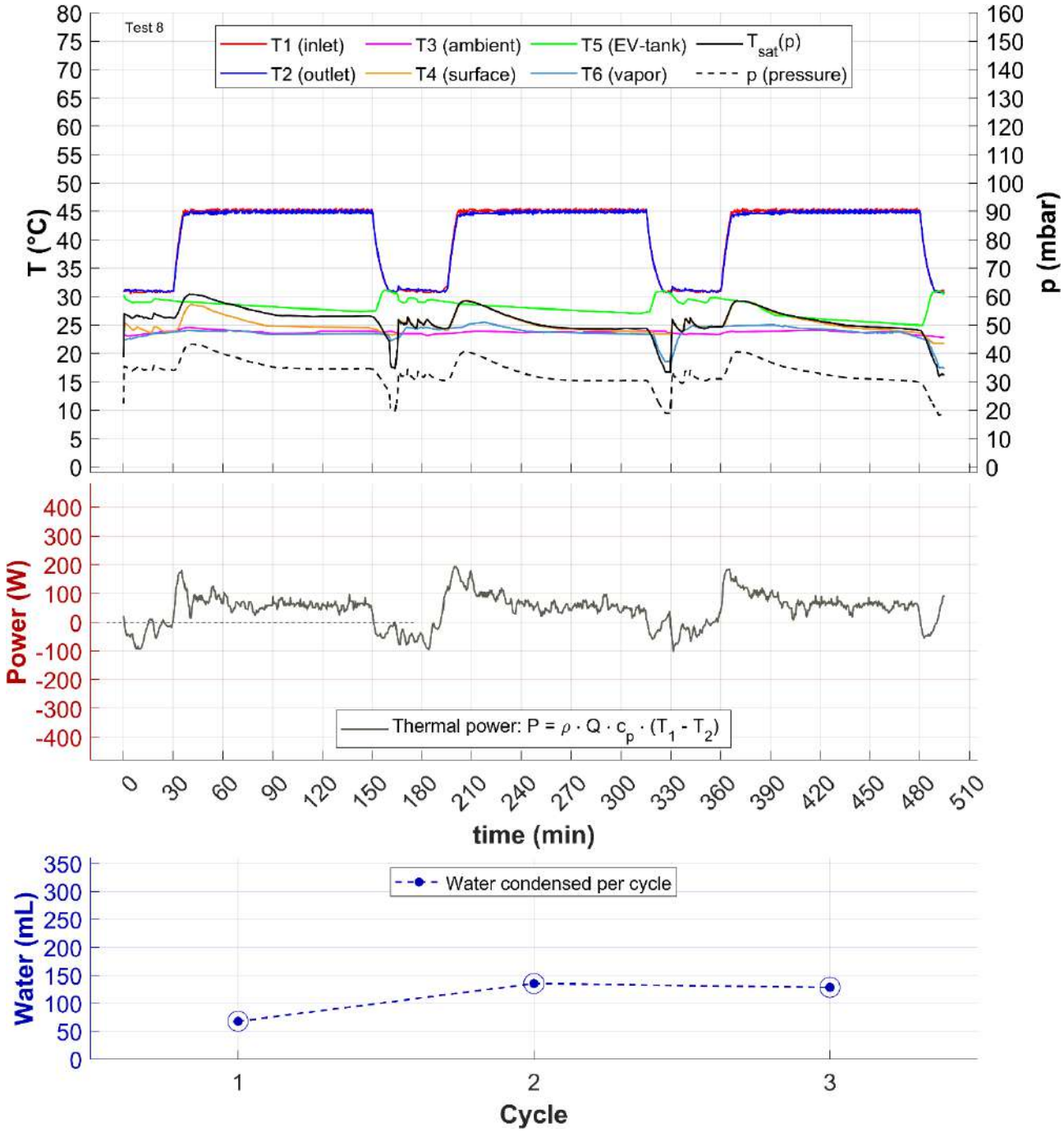

Figure s9: Test 8, material: Silica-gel, TADS: 30°C, tADS: 30 min, TDES: 45°C, tDES: 120 min. Sensor T6 (vapor) was not included in the main discussion, given the redundant information it gives with respect to T3. 'p' is vapor pressure in the adsorber.

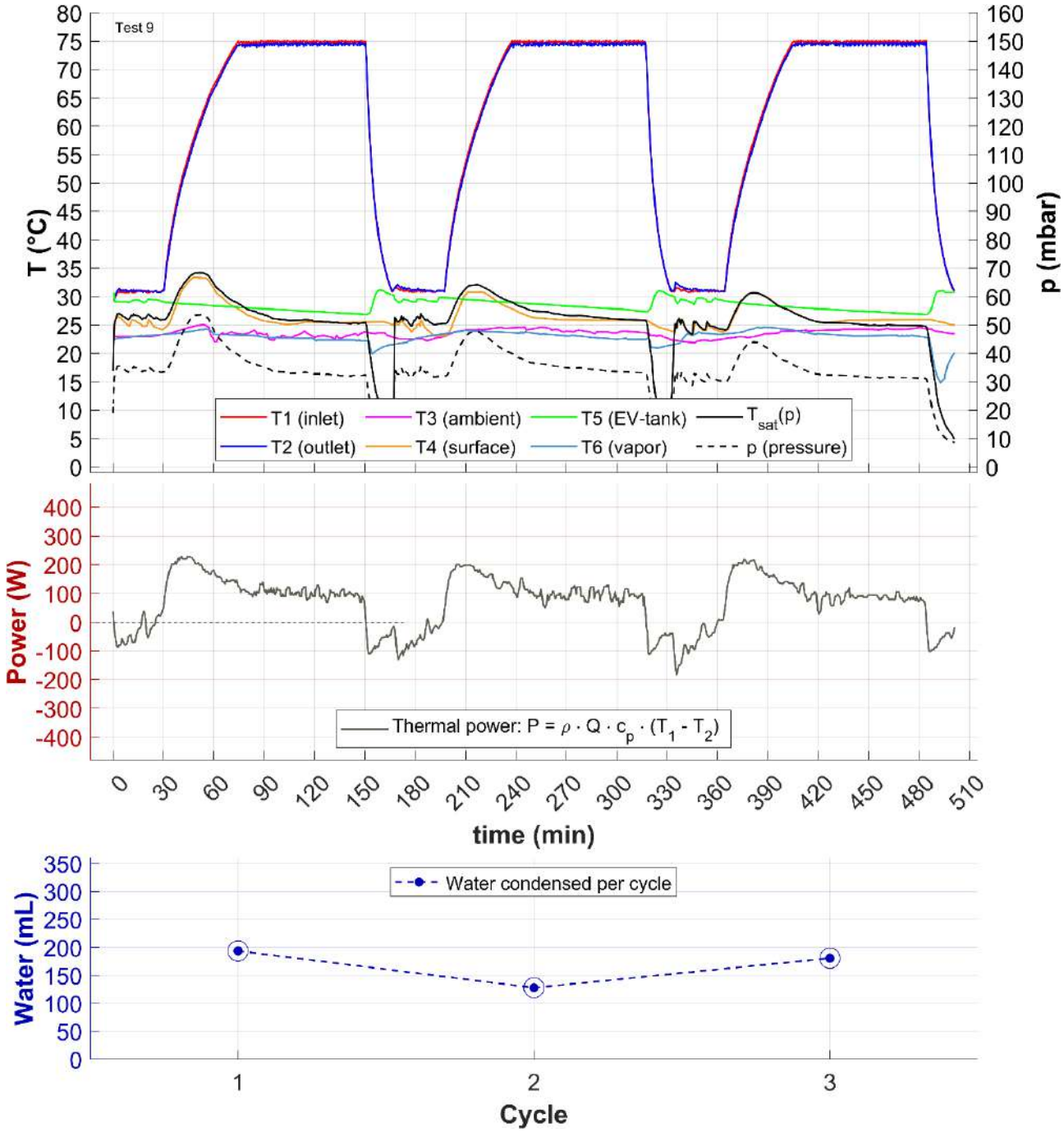

Figure s10: Test 9, material: Silica-gel, TADS: 30°C, tADS: 30 min, TDES: 75°C, tDES: 120 min. Sensor T6 (vapor) was not included in the main discussion, given the redundant information it gives with respect to T3. 'p' is vapor pressure in the adsorber.

Note S5 – Residual salt in the condensed water

Possible reasons for the residual salt concentration in the collected water are here proposed.

1. The internal surfaces of the machine might be contaminated. Indeed, even when performing tests starting from distilled water (8 µS/cm), higher conductivity in the collected water was measured (85 µS/cm), both when testing CaAlg and when testing silica-gel. The EV tank internal surface itself was found to contaminate resting water, bringing conductivity from 8 µS/cm to 22 µS/cm even outside of tests.
2. Some liquid water drops (aerosol) migrated from the EV tank into the adsorber (most probably at the beginning of the adsorption phase, with a large pressure difference between the two chambers). This is proven by the fact that some residual salt tracks were found on the side surface of the exchanger after the test with salty water (Fig. s11).

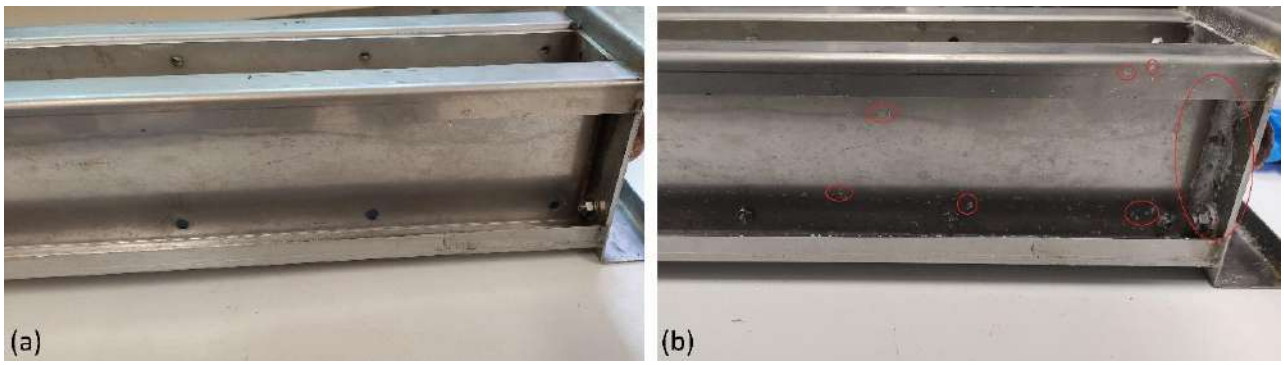

Figure s11. a, exchanger before the test with salty water. b, Exchanger after the test with salty water (some of the salt tracks are circled in red).

The second point above raises the question of how much the migrated amount of water, together with the water condensed on the adsorber vessel walls during the adsorption phase, contributes to the collected amount at the end of the cycles. In order to answer, a further test was conducted, where, during the desorption phase, the material was not heated, but the V3 valve was opened: this allowed approximately 30 mL of water to be collected. Such amount is surely much smaller than the amounts of water collected when proper desorption is carried out (most of the times ranging from 100 mL to 200 mL, depending on the specific tests conditions), thus it does not invalidate the qualitative considerations made, but it is still important to consider for future improvements in the system.

Note S6 – Water analysis

In order to preliminarily test the ability of the hydrogel to work with a salty solution, few cycles using salty water were performed after the main experimental campaign, with adsorption temperature of 30°C, adsorption time of 30 min, desorption temperature of 60°C, desorption time of 75 min. To this end, a salty solution of water and NaCl at a concentration of 3.5% w/w (simulating sea water [S12]) was prepared. The solution was positioned in the EV tank. The water level was not monitored cycle by cycle as for the main campaign, but part of the condensed water was collected and analysed, together with other water samples: one sample of distilled water, one of distilled water after stationing in the EV tank, one of salty "sea" water, one of condensed water starting from distilled water, and most importantly one of condensed water starting from salty "sea" water. The detailed list of samples and measurements is reported below (Table s4).

For each collected water sample the following experimental measurements were performed:

- Conductivity (μS/cm). Sensor RS PRO 1410 was used, with accuracy of 1 μS/cm.
- Residual solid content (mg/L). Sensor RS PRO 1410 was used, with resolution of 1 mg/L (the tool uses an estimated default conversion formula to convert conductivity into salt concentration). In the case of samples #3 and #5, a thermobalance KERN DBS60-3 (accuracy 0.001 g) was used to evaporate the solutions at 180°C for 5 hours and confirm the estimation.
- PH. The sensor DrMeter-PH838 (accuracy of 0.05 PH) was used.
- Presence of organic compounds. A TOC (Total Organic Carbon) analysis was performed, from which Total Carbon and Inorganic Carbon were measured and the TOC was evaluated. Analyses were performed by the DIATI department at Polito, with total organic carbon (TOC) analyser LCSH FA (Shimadzu, Italy; catalytic oxidation on Pt at 680 °C).
- Presence of copper (Cu). Analyses were performed by the DIATI department at Polito, with ICP-MS (inductively coupled plasma-mass spectrometry) by ThermoScientific (model iCAP RQ), using kinetic energy discrimination (KED).

Sample #	*Description*	*Solid content (mg/L)*	*Conductivity at 20°C (μS/cm)*	*PH*	*TOC (ppm)*	*Inorganic Carbon (ppm)*	*Copper (ppb)*
1	Distilled water	8	8	5.4	1.13	0.549	5.77
2	Distilled water after standing in the EV tank	23	22	5.6	n.a.	n.a.	n.a.
3	"Sea water"	34500	50700	5.6	< 3.43 *	n.a. *	1.54
4	Condensed water starting from sample #2	93	85	5.7	n.a.	n.a.	n.a.
5	Condensed water starting from sample #3	274 ± 35 **	245 ± 32 **	7.9 ± 0.1 **	6.80 ± 5.7 **	1.77 ± 0.51 **	7.03 ± 2.2 ***
6	Commercial water for reference "LEVISSIMA naturale"	157	144	7.0	n.a.	n.a.	n.a.

*n.a.: not available. * The measurement of Inorganic Carbon for this sample is not available. The reported value "3.43 ppm" is the Total Carbon, an overestimation of the TOC. ** Average ± standard deviation on 3 samples. *** Average ± standard deviation on 2 samples.*

Table s4: Solid content, conductivity, PH, TOC, Inorganic carbon and copper content for the analysed water samples.

For what concerns PH, the measured value is always contained within the range 4.5-9.5. The World Health Organization does not propose health-based guidelines for the PH value in drinkable water. Nevertheless, further investigation is suggested to understand whether the apparent increase in PH

between the starting salty water and the condensed clean water may indicate that some compound dissolved in the process.

For what concerns the organic content, a carbon analysis was made. This allowed to estimate the TOC (Total Organic Content) as well as the Inorganic Carbon present in the water samples. An increase in the Total Carbon was seen between the starting salty water (sample 3, with 3.43 ppm) to the final condensed clean water (sample 5, with 8.57 ppm, of which about 6.8 ppm are net TOC). On the other hand, an increase in the Total Carbon was seen between the distilled water (sample 1, with Total Carbon of 1.68 ppm) and the salty water (sample 3, before being processed by the sorbent, with 3.43 ppm), too. This shows that the contamination in the testing environment was high, and comparable to the measured amounts: looking at the orders of magnitude of the measured quantities, it is probable that a fraction of the TOC in sample 5 derives from unwanted contamination in the machine, unrelated to the use of calcium alginate. To have a better picture and understand whether the CaAlg releases organic compounds in the condensed water, further testing in a more controlled testing environment is necessary.

For what concerns copper, the metal is never present in sensible amounts. This shows that there is no contamination from the heat exchanger copper parts.

For what concerns conductivity, an actual desalination effect was indeed achieved: the condensed water had a conductivity of 245 µS/cm, that, compared with the starting conductivity of 50700 µS/cm of the water in the EV tank simulating the sea salinity, shows a useful reduction of over 99.5%. The estimated solid content in mg/L reduced by a similar amount, 99.2%. The reduction of solid content was confirmed by a regular solid content evaluation test in thermal balance (Fig. s12).

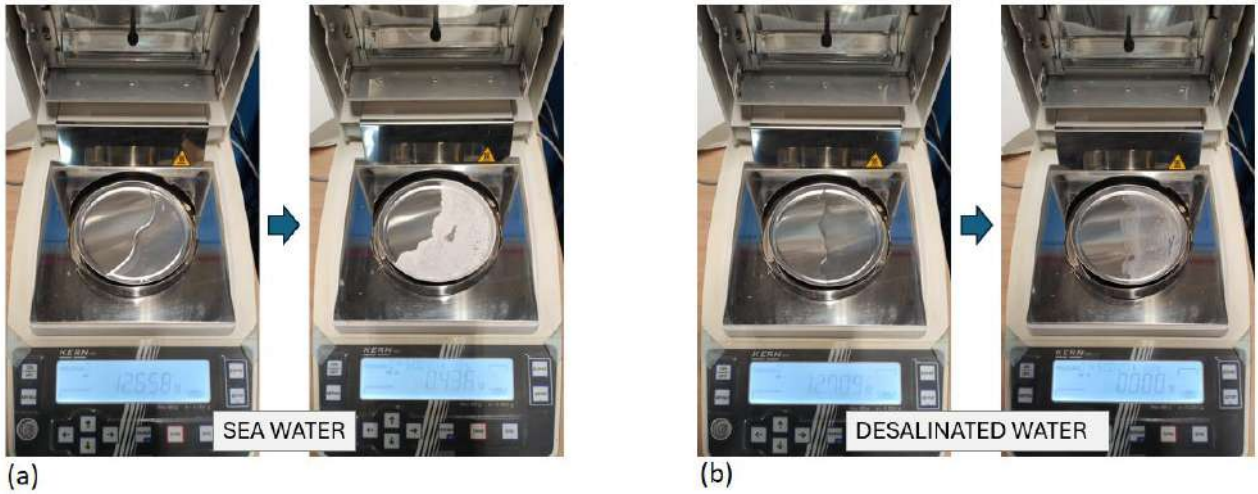

Figure s12. a, After evaporating 12.658 g of salty water from sample #3 at 180°C for 5 hours, the residual solid content is 0.436 g, thus confirming an initial 'sea water' salinity of 3.4-3.5 % w/w. b, After evaporating 12.709 g of desalinated water from sample #5 at 180°C for 5 hours, the residual solid content is below the scale resolution.

The thermodynamical variables during the test with salty water (Fig. s13) behaved similarly as in the tests with distilled water.

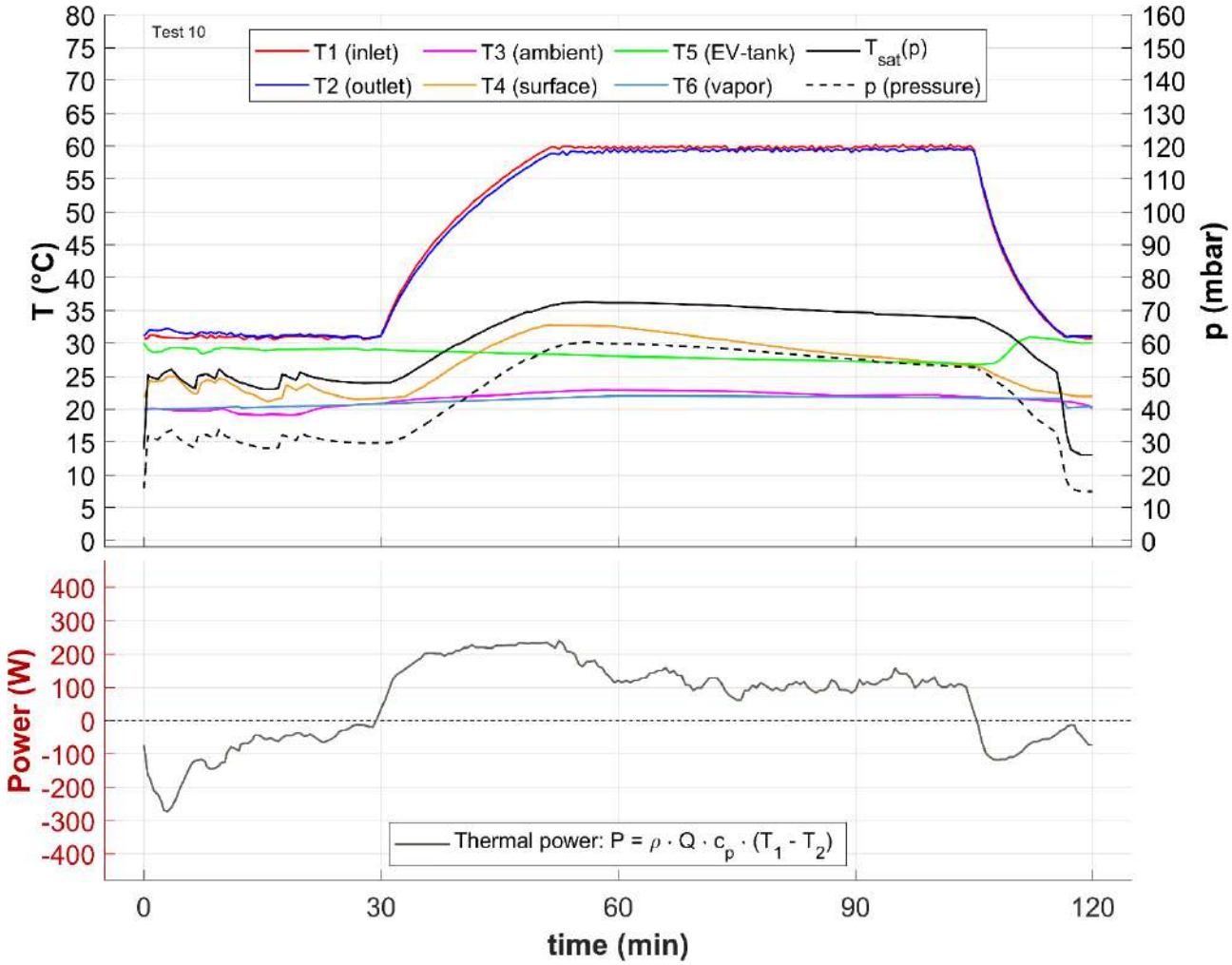

Figure s13: A cycle with 'sea water' as feedwater. Material: CaAlg, TADS: 30°C, tADS: 30 min, TDES: 60°C, tDES: 75 min. Sensor T6 (vapor) was not included in the main discussion, given the redundant information it gives with respect to T3. 'p' is vapor pressure in the adsorber.

Note S7 – Kinetics and estimation of diffusivities

The data collected with the ProUmid analyser allows to discuss the dynamic behaviour of the material in the adsorption and desorption transients. In Fig. s14a the charging and discharging ramps of the sample of CaAlg 'after 40 cycles' are shown, for the RH range 20%-70%: on the horizontal axis, the test time; on the vertical axis, the water uptake. Pictures of the sample are shown with the CaAlg in equilibrium at RH=20% (Fig. s14c), RH=40% (Fig. s14d), RH=70% (Fig. s14e).

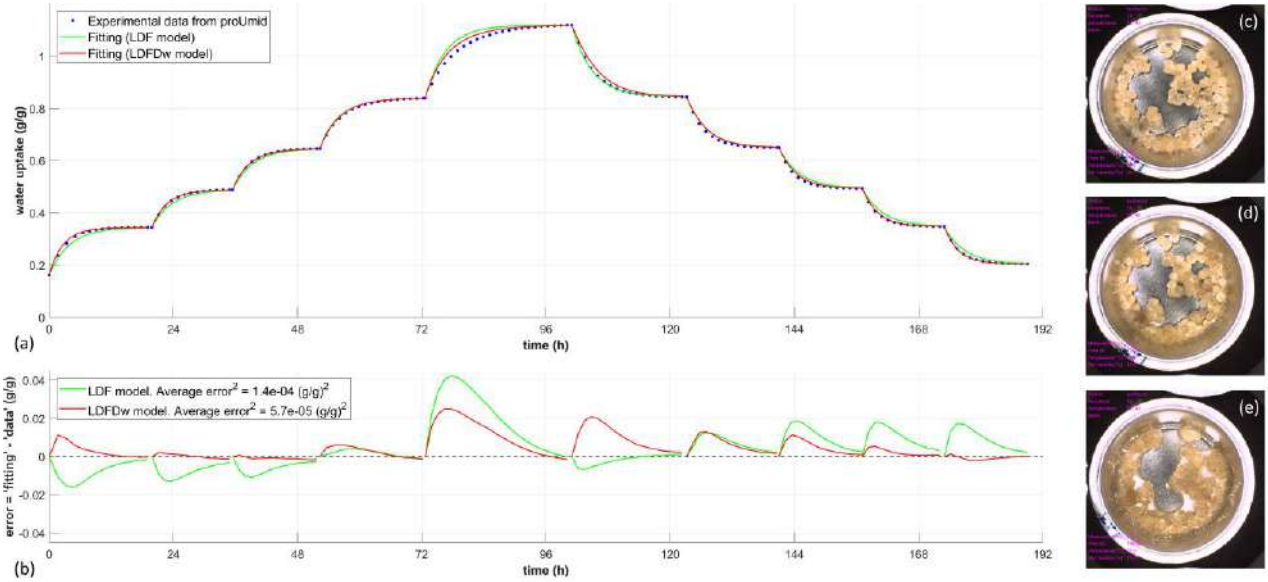

Figure s14. a, Water uptake of sample CaAlg 'after 40 cycles' during Experiment A, with T=30°C and RH ranging between 20% and 70%, compared with LDF and LDFDw best-fittings. b, Absolute error made by the two models. c, Sample appearance at RH=20%. d, Sample appearance at RH=40%. e, Sample appearance at RH=70%, showing salt deliquescence.

Once a proper adsorption model is identified, the experimental data can be best-fitted (e.g., by least-squares method) and the model parameters can be found. In this case, this was done with two available models (see main text for details), whose expressions are here provided for convenience:

- LDF model:

$$w(t) = w_0 + (w_\infty - w_0) \cdot \left(1 - e^{-\frac{F_0 \cdot D}{R_p^2} \cdot t}\right)$$

- LDFDw model:

$$w(t) = \frac{e^{\frac{F_0 \cdot (a + b \cdot w_{eq})}{R_p^2} \cdot t} - 1}{e^{\frac{F_0 \cdot (a + b \cdot w_{eq})}{R_p^2} \cdot t} + b \cdot \left(\frac{w_{eq} - w_0}{a + b \cdot w_0}\right)}$$

Being the LDFDw a generalization of the LDF model using one further parameter, the best-fitting is clearly better (with the drawback of having a more complex expression for D), as proved in the Fig. s14b, where the errors made over time by the two models are compared. The result of the least-squares-fitting in the two cases is the following:

$$\begin{aligned} &LDF: && D = D_{30°C} = 2.6733 \cdot 10^{-12} && m^2/s \\ &LDFDw: && D = D_{30°C} = 4.4399 \cdot 10^{-12} - 2.2985 \cdot 10^{-12} \cdot w && m^2/s \end{aligned}$$

These coefficients, modelling the diffusivity at 30°C, are used for the simulations in Supplementary 12. It is worth considering that the characterization in the ProUmid analyser has been carried out under positive pressure and the resulting diffusivities might be affected by factors such as:

- presence of gas molecules in the chamber, which might slow down mass transfer;
- change in the geometry of the beads and in the porosity size happening under vacuum;
- forced convection in the ProUmid analyser chamber (the supplier estimates a gas velocity in the chamber of 0.3 m/s).

In Table s5 the fitting results for all the tested samples are reported. In general, the diffusivities estimated via LDF model for CaAlg are similar, ranging from $1.96 \cdot 10^{-12}$ m^2/s to $3.21 \cdot 10^{-12}$ m^2/s depending on the specific sample. These values are similar to the ones provided in the Literature for similar compositions ($2.7 \cdot 10^{-12}$ m^2/s for composition Alg_1Ca_5 [S13]). The LDFDw model estimates similar values as well, but shows that a better fitting is got if diffusivity at 30°C is considered decreasing with the amount of water adsorbed by the material. On the other hand, silica-gels diffusivities are estimated to be greater by both models, reaching $1.38 \cdot 10^{-11}$ m^2/s for the mesoporous material. As a reference, in the literature values of the order of magnitude of 10^{-11} m^2/s are proposed [S 14,15].

#	Sample	*LDF model (D=constant)*	*LDFDw model (D=a+bw)*	
		D (m^2/s)	*a (m^2/s)*	*b (m^2/s)*
1	CaAlg-P1 'as produced'	2.3165e-12	3.8539e-12	-1.9338e-12
2	CaAlg-P1 'as produced'	1.9602e-12	3.1908e-12	-1.5355e-12
3	CaAlg-P1 'as produced'	2.0970e-12	3.4669e-12	-1.7101e-12
4	CaAlg-P2 'as produced'	2.9736e-12	5.2914e-12	-2.9004e-12
5	CaAlg-P2 'as produced'	3.2148e-12	5.7963e-12	-3.1579e-12
6	CaAlg-P2 'as produced'	2.1791e-12	3.8598e-12	-2.0775e-12
7	CaAlg-P1 'after 20 cycles'	2.9922e-12	5.1280e-12	-2.8659e-12
8	CaAlg-P2 'after 20 cycles'	2.8662e-12	4.8607e-12	-2.5662e-12
9	CaAlg-P1 'after 30 cycles'	2.5994e-12	4.3916e-12	-2.3856e-12
10	CaAlg-P2 'after 30 cycles'	2.4104e-12	3.9398e-12	-2.0154e-12
11	CaAlg-P1 'after 40 cycles'	2.6270e-12	4.3621e-12	-2.3303e-12
12	CaAlg-P2 'after 40 cycles'	2.6733e-12	4.4399e-12	-2.2985e-12
13	Silica-gel 'microporous'	3.7031e-12	4.1324e-12	-3.3240e-12
14	Silica-gel 'mesoporous'	8.7188e-12	1.3778e-11	-2.4067e-11

Table s5: Samples diffusivities at 30°C according to a least-squares fitting with LDF and LDFDw model.

The higher diffusivity for silica-gel samples suggests that the CaAlg has a slower adsorption kinetics. This is important to know, since this might be compensated by the larger equilibrium uptake only if long cycles are performed: in the case short cycles are required by the application, like for adsorption chillers, the silica-gel may remain the best choice. Further investigation is needed to understand what happens when the adsorption time is reduced. A different setup shall be built for the scope though, since, given the design limitations, shorter cycles times in the used prototype would be comparable with the transient times of the heating/cooling external circuits, not allowing significant tests.

Note S8 – Synthesis of CaAlg

We report here the production procedure followed for Calcium Alginate. First, a solution of NaAlg and distilled water 1% w/w (weight of solute / weight of solution) is prepared; this is dripped in a second solution of $CaCl_2$ and distilled water 10% w/w, and the drops start jellifying in the shape of pseudo-spherical beads as soon as the two liquids come in contact (fig. s15a).

The used distilled water has a conductivity of ~8 µS/cm. The NaAlg and CaAlg come from suppliers *Carlo Erba Reagents* and *Alquera*, respectively. The chosen chemicals concentrations of 1% for NaAlg and 10% for CaAlg in their corresponding solutions are suggested from previous optimization studies [13]. Considering a purity for the used $CaCl_2$ of 77% as specified by the supplier, the actual content of salt in the second solution can be estimated to be approximately 8% w/w.

This was experimentally confirmed *a posteriori*: 3.202 grams of well-mixed $CaCl_2$ solution were collected before the production process, 3.148 grams more were collected after the production process, and a thermal balance (KERN DBS60-3, with accuracy of 0.001 g) was used to evaporate the two water samples separately at 180 °C for 5 hours, as in the standard procedure suggested to measure the total dissolved solids in a water solution. The final amounts of residual salt were, respectively, 0.271 g and 0.241 g, corresponding to 8.46% and 7.66% w/w concentration. Then, it can be safely assumed that all the jellification process happened in a $CaCl_2$ solution having 8.0 % ± 0.5% salt concentration. Using the same nomenclature as in Gentile et al (2024), the produced CaAlg composition can be thus identified as "Alg_1Ca_8" [S 13].

The production setup built to synthetize the material follows the same idea as in Gentile et al (2024). It consists of a series of plastic tanks and pipes positioned within an aluminium frame and used to contain the solutions, a mixer used to homogenise the liquids, and a peristaltic pump used to move a constant flow-rate of viscous NaAlg solution through three 3D-printed nozzles having 1.8 mm diameter each: the drops fall by gravity from a height of ~30 cm and directly onto the surface of the $CaCl_2$ solution, where the formed beads are moved by turbulence to the sides of the $CaCl_2$ solution container. Here, they are collected at the end of the procedure (Fig. s15b).

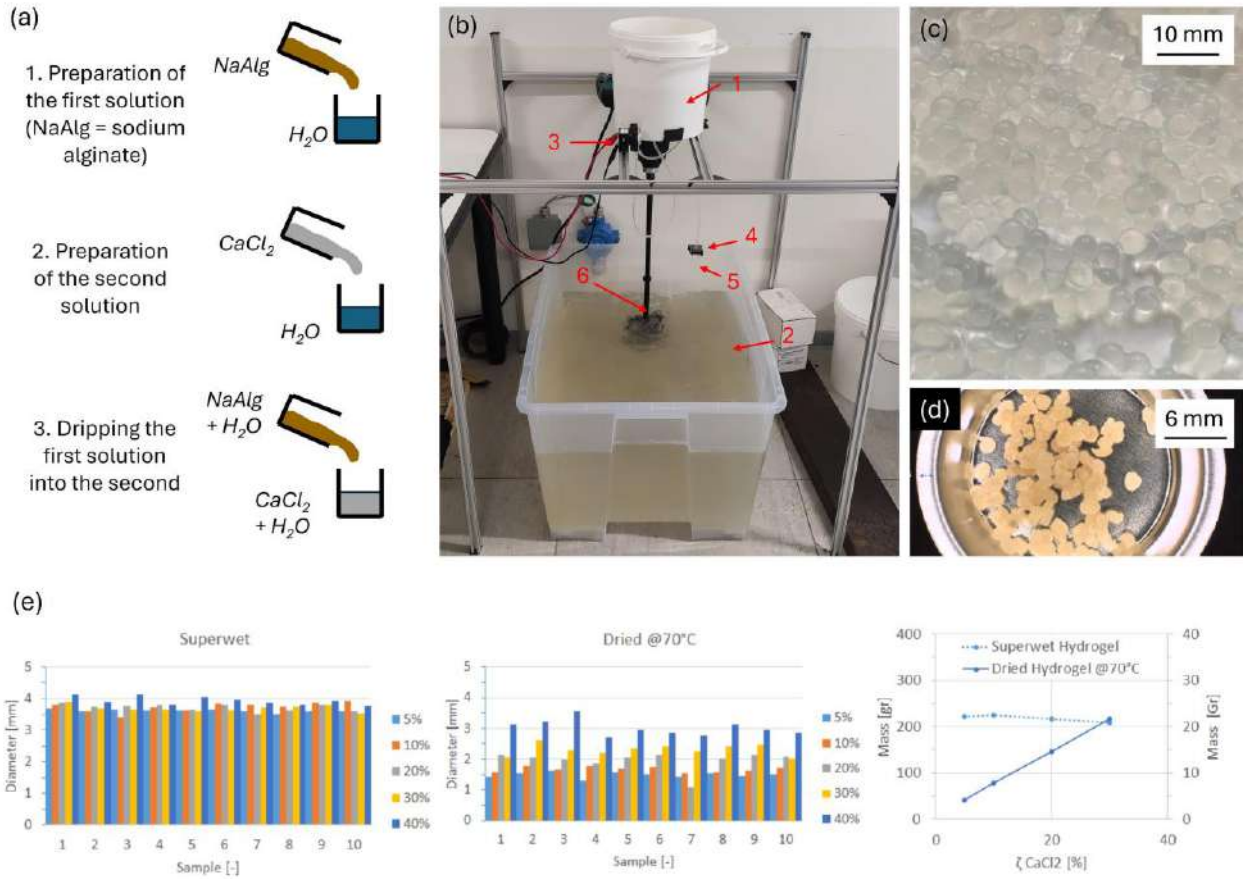

Figure s15. a, Hydrogel production steps. b, Setup built for the material production (1: Container with NaAlg solution; 2: container with $CaCl_2$ solution; 3: peristaltic pump; 4: nozzle; 5: NaAlg drops; 6: mixer). c, CaAlg beads after the jellification; d, CaAlg beads after the drying process at 75°C in a ventilated oven. e, Change in "superwet" and "dried" beads diameter and mass as a function of $CaCl_2$ concentration [S 16].

After jellification begins, the beads are left in the $CaCl_2$ solution for 12 hours to complete the polymerization process. At this point, the produced material is in the shape of spherical beads with diameter of 3-6 mm (Fig. s15c), containing a large amount of water that should be removed before the material can be used. For this reason, the spherical beads are dried in a ventilated oven at 75°C, at the end of which they appear smaller and yellowish (Fig. s15d).

Figure s15e shows the influence of $CaCl_2$ concentration during ionotropic gelation, while keeping other parameters constant (H_2O/NaAlg ratio, gelation period and duration, regeneration temperature and time) [S 16]. The volumetric shrinkage of the beads and the mass reduction of the batch are associated with water loss from the initial composition and are inversely proportional to $CaCl_2$ concentration. According to the literature, network formation in alginate chains occurs in three main steps: i) interaction of Ca^{2+} ions with single guluronate units forming mono-complexes; ii) propagation and formation of egg-box dimers through pairing of these mono-complexes; iii) lateral association of dimers into multimers. An increase in Ca^{2+} concentration enhances the probability of multimer formation, resulting in a higher amount of bound Ca^{2+} and a greater likelihood of trapping fillers (e.g., solvated $CaCl_2/H_2O$ complexes) within parallel chains. Both effects lead to higher batch mass, larger bead volume, and increased internal porosity and polymer chain complexity [S17,18,19].

Note S9 – Desalination unit components

Component	*Type*	*Scope*	*Description*
T1	Sensor	Monitoring water temperature at the inlet of the adsorber (external orange loop).	Class-A PT1000. Accuracy: ±0.3 °C.
T2	Sensor	Monitoring water temperature at the outlet of the adsorber (external orange loop).	Class-A PT1000. Accuracy: ±0.3 °C.
T3	Sensor	Monitoring ambient temperature.	Class-A PT1000. Accuracy: ±0.3 °C.
T4	Sensor	Monitoring temperature of the external surface of the adsorber vessel.	Class-A PT1000. Accuracy: ±0.3 °C.
T5	Sensor	Monitoring water temperature in the EV tank (under vacuum).	Class-A PT1000. Accuracy: ±0.3 °C.
p	Sensor	Monitoring vapor pressure in the adsorber (under vacuum).	JC627CA-3A1F3W3 absolute pressure sensor, 0-200 mbar. Accuracy: ±0.5 mbar.
Q7	Sensor	Monitoring water flow (external orange loop).	Hall-effect type flowmeter, with range 2-100 L/min, model YF-G1. Accuracy: ±5%.
V2	Actuator	Opening/closing the vapor passage between the EV water tank and the adsorber.	Electric valve, internal diameter 20 mm. Opening/closing time: 20 s.
V3	Actuator	Opening/closing the vapor passage between the adsorber and the CD water pipe.	Electric valve, internal diameter 20 mm. Opening/closing time: 20 s.
VA	Actuator	Allowing water replacement in the EV tank.	Manual valve, internal diameter 25 mm.
VB	Actuator	Allowing water collection from the CD pipe.	Manual valve, internal diameter 25 mm.
P6	Actuator	Circulating water in the EV (external magenta loop).	IBO OHI15-60/130 pump, peak consumption of 93 W.
H6	Actuator	Providing the power to heat up the EV water during evaporation (external magenta loop).	SKU800T electric heater, peak consumption of 1800 W.
F16	Actuator	Dissipating the heat to cool down the EV water (external magenta loop).	Size 30x9x35 cm, air velocity of 4.0 m/s.
P7	Actuator	Circulating water in the adsorber (external orange loop).	IBO OHI15-60/130 pump, peak consumption of 93 W.
H7	Actuator	Providing the power to heat up the sorbent during desorption (external orange loop).	SKU800T electric heater, peak consumption of 1800 W.
F17	Actuator	Dissipating the heat to cool down the sorbent during adsorption (external orange loop).	Size 30x9x35 cm, air velocity of 4.0 m/s.
F18	Actuator	Dissipating the heat of condensation, cooling down the adsorber vessel surface.	Fan, electric consumption of 33 W. Air velocity at the vessel surface: 1.42 m/s.
A6	Accessories	Safety hydraulic equipment.	Expansion vessel, safety valve calibrated at 3.0 bar, manometer, air vent valve, manual tap for filling and emptying of the circuit.
A7	Accessories	Safety hydraulic equipment.	Expansion vessel, safety valve calibrated at 3.0 bar, manometer, air vent valve, manual tap for filling and emptying of the circuit.

Table s6: Desalination unit components.

Note S10 – Description of tests in the ProUmid analyser

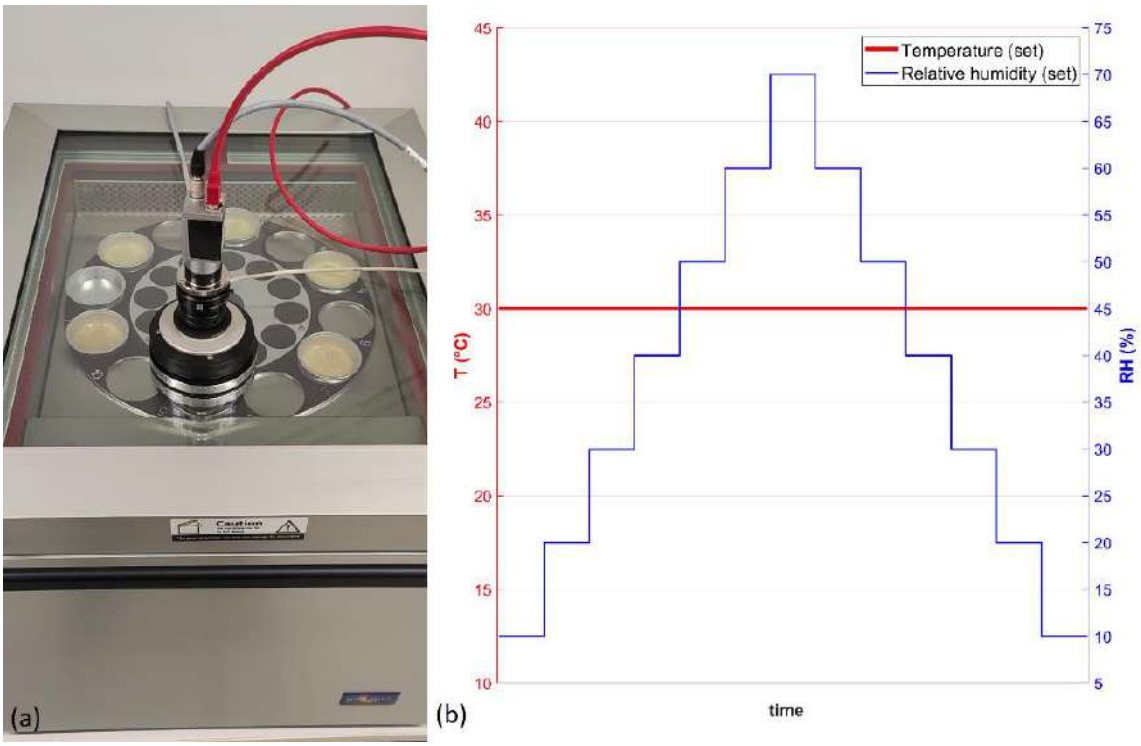

Figure s16. a, Picture of the ProUmid analyser. b, The set conditions for T (left y-axis) and RH (right y-axis) for the isotherm preparation; the time axis is qualitative, since the duration of each ramp depends on the reaching of the equilibrium conditions: the actual experiment lasted in total approximately 14 days.

#	*Sample*	*Description*
1	CaAlg-P1 'as produced'	Sample I of virgin CaAlg from production P1.
2	CaAlg-P1 'as produced'	Sample II of virgin CaAlg from production P1.
3	CaAlg-P1 'as produced'	Sample III of virgin CaAlg from production P1.
4	CaAlg-P2 'as produced'	Sample I of virgin CaAlg from production P2.
5	CaAlg-P2 'as produced'	Sample II of virgin CaAlg from production P2.
6	CaAlg-P2 'as produced'	Sample III of virgin CaAlg from production P2.
7	CaAlg-P1 'after 20 cycles'	Sample of CaAlg from production P1 after 20 cycles.
8	CaAlg-P2 'after 20 cycles'	Sample of CaAlg from production P2 after 20 cycles.
9	CaAlg-P1 'after 30 cycles'	Sample of CaAlg from production P1 after 30 cycles.
10	CaAlg-P2 'after 30 cycles'	Sample of CaAlg from production P2 after 30 cycles.
11	CaAlg-P1 'after 40 cycles'	Sample of CaAlg from production P1 after 40 cycles.
12	CaAlg-P2 'after 40 cycles'	Sample of CaAlg from production P2 after 40 cycles.
13	Silica-gel 'microporous'	Sample of microporous silica-gel (Oker Chemie, grain size of 0.5-1.5 mm)
14	Silica-gel 'mesoporous'	Sample of mesoporous silica-gel (Oker Chemie, grain size of 1.5-3.15 mm)

Table s7: List of the samples tested for the complete isotherm. The suffixes "-P1" and "-P2" are used to differentiate between two batches of production, among which no significant difference was seen. The results in the main text refer to batch 'P2'. The error bars in Fig. 2a and Fig. 2c are evaluated by reporting on sample 12 the uncertainty seen from the measurements on samples 4, 5 and 6.

Note S11 – Dependence of adsorption enthalpy by isotherm offset

Starting from the point at RH=10% and extending linearly the isotherm in the range 0-10% (assuming the same slope as in the range 10-20%), the isotherm intersects the y-axis at the value of: "$-0.1622\ g/g$". If the original isotherm is shifted up by $w^* = 0.1622\ g/g$, the new 'adjusted' curve intersects the origin of the axes (that is, $w = 0\ g/g$ at $RH = 0\ \%$), and it becomes comparable with data from literature (Fig. s17a).

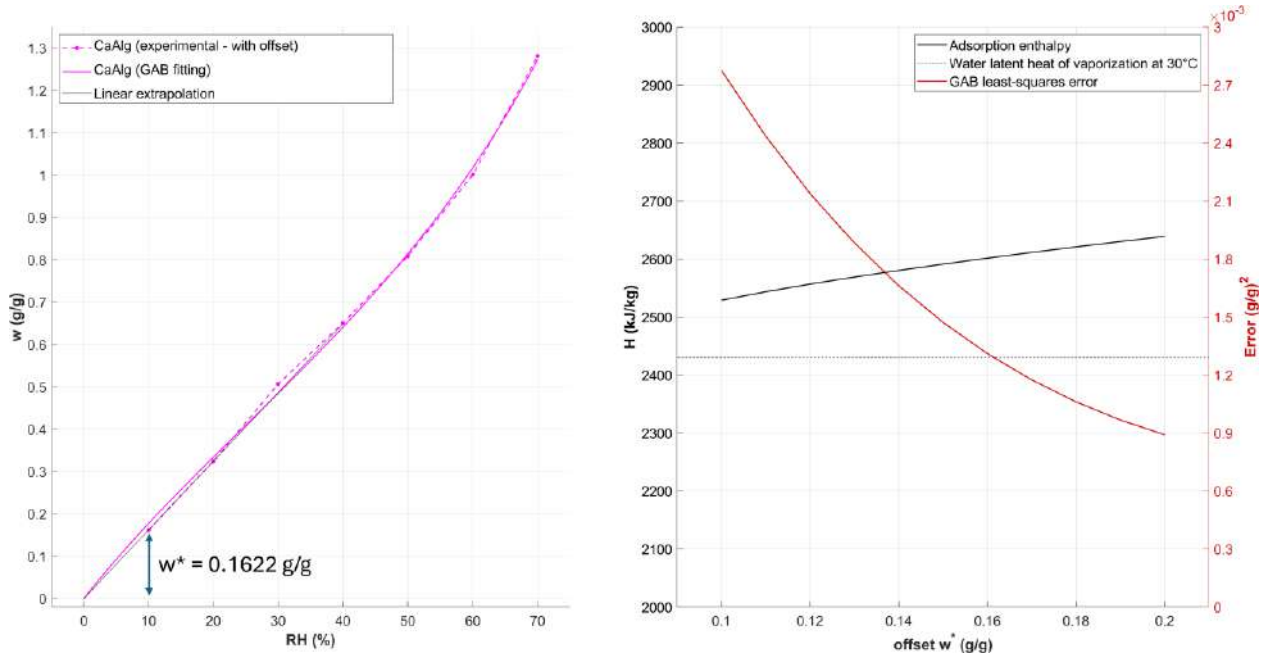

Figure s17. a, CaAlg 'after 40 cycles' isotherm with offset w, compared with the GAB model. b, Adsorption enthalpy and GAB fitting error as a function of the arbitrary offset.*

The offsetting procedure is clearly arbitrary: in reality, it is not possible to know how lower the equilibrium value at RH=0% would have actually been without performing a proper experiment. Using the GAB model on the original data is not possible, too: by the model definition, at RH=0% the uptake is equal to 0%, which is not compatible with the experimental data (an attempt of fitting the GAB or the BET model with the original data was made, and resulted in values for the fitted coefficient out of the range for which the model is significant). An alternative to the proposed procedure would be to keep the original data and add an offset coefficient w* to the GAB model, making it a 4-parameters expression: the result would be identical, though, with the cons that the isotherm would still be not comparable with other data from literature.

Since the choice of the offset was arbitrary, for completeness, in Fig. s17b it is shown what would happen by choosing a different offset value in the range 0.1-0.2 g/g. Increasing w*, the error of the GAB fitting decreases and Hads increases, but with a sublinear rate. For instance, by using an offset of 0.12 g/g instead of 0.1622 g/g, the value of Hads changes by 1.8% (2557 kJ/kg instead of 2604 kJ/kg). For what concerns the comparison with the other isotherms from literature: the shape of the isotherm is not changed by applying the offset, so the qualitative considerations are still valid. The equilibrium values are instead modified, but not in such a way to affect the relative position of the isotherm with respect to the samples from literature (even without applying any offset, the equilibrium value at RH=70% is still larger than the other analyzed samples), thus the discussion in the main text is still valid.

Note S12 – Simulation of SDWP

In Fig s18a we report a full day of cycling of a CaAlg simulated through the model LDFDw. As for the diffusivity at 30 °C (which was used to simulate adsorption), the experimental curves obtained with the ProUmid analyser were best-fitted (Supplementary 7) and the resulting expression $D_{30°C} = a + b \cdot w$ is used, with $a = 4.4399 \cdot 10^{-12}\ m^2/s$ and $b = -2.2985 \cdot 10^{-12}\ m^2/s$. For the diffusivity $D_{60°C}$ at 60°C (which was used to simulate desorption), since no experimental data was available, it was assumed $D_{60°C} = 2 \cdot D_{30°C}$, following the results obtained in [S13] for a similar composition.

As for the equilibrium values to run the models: for adsorption at 30°C it was used $w_{ads,eq} = 1.12\ g/g$ (that is the value suggested by the isotherms before the offsetting procedure, see Supplementary 11); for desorption, since no isotherm at 60°C was available, it was assumed $w_{des,eq} = 0.00\ g/g$ (the implications of this assumption are discussed below).

For the simulation, the adsorption time and temperature are fixed at 30 min and 30°C respectively, while the desorption temperature is fixed at 60°C, to replicate the conditions in the desalination unit. The desorption time is chosen among 10 min, 30 min and 120 min, and the evolution of the uptake in the material along multiple successive cycles over the day is simulated.

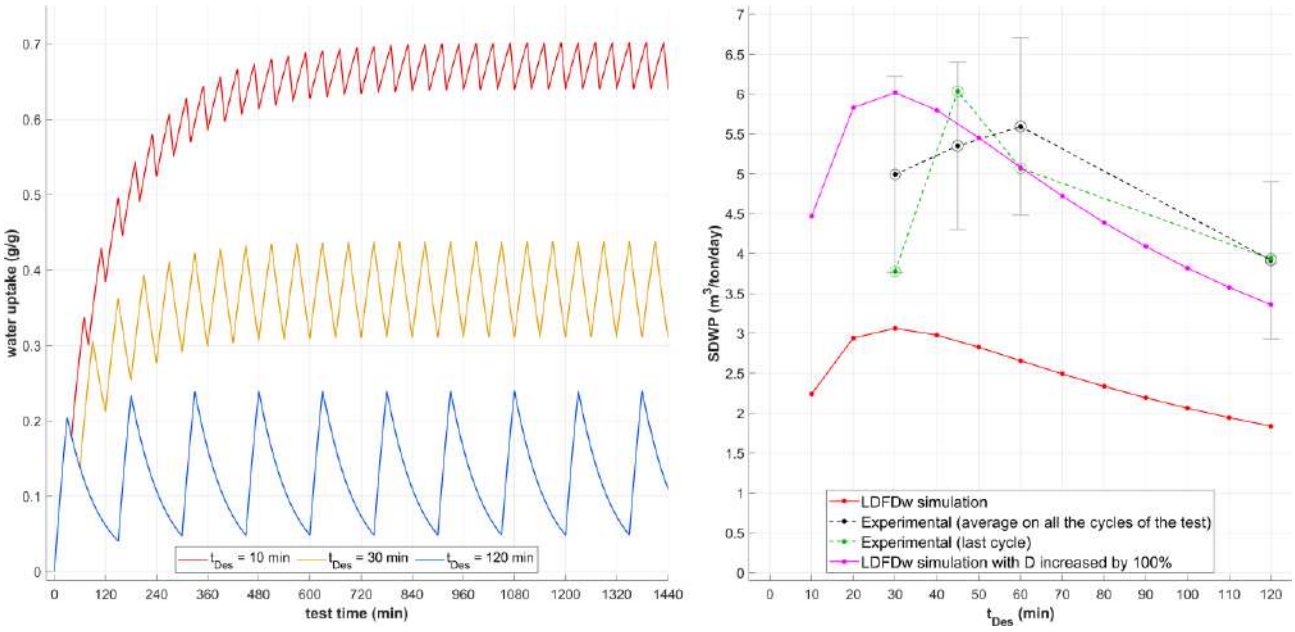

Figure s18: a, Numerical simulation of 24 hours of repetitive cycling with CaAlg beads, at different desorption times but fixed adsorption time, adsorption temperature and desorption temperature; the model LDFDw was used. b, Simulated vs experimental SDWP as a function of desorption time t_{Des}.

The red curve in Fig. s18a refers to the shortest simulated desorption time, 10 min: after some initial cycles (the amount of which depends on the initial state of charge of the material, here assumed to be 0.0 g/g), the uptake oscillations stabilize in the range 0.6404-0.7026 g/g. Such values are compatible with the chosen adsorption and desorption times, in such a way that at the end of a full adsorption-desorption cycle the uptake is again the same as it was at the beginning of the cycle. In this case, the cycle time (excluding pre-cooling) equals to 40 minutes (30 min adsorption + 10 min desorption), and the theoretical SDWP can be evaluated as: $SDWP = \frac{0.7026\ mL/g - 0.6404\ mL/g}{40\ min\ /\ 60\ min} \cdot 24\ h = 2.24\ mL/day/g\ = 2.24\ m^3/day/tons$.

The yellow curve in Fig. s18a refers to an intermediate desorption time, 30 min: here the cycle time is longer (1 h), but even greater is the difference in the two uptakes between which the material charge oscillates, from which a SDWP of $3.06\ m^3/day/tons$ (larger than in the previous case) follows.

The blue curve in Fig. s18a refers to the case where the desorption time is 2 h long: in this case, the SDWP decreases down to $1.84\ m^3/day/tons$, because the benefit of greater water production is not compensated by the increase of length of the cycle.

The procedure can be repeated for a denser range of desorption times, and an optimal SDWP as a function of desorption time can be found. This is shown here for desorption times ranging from 10 to 120 minutes in 10-min steps in the red curve on Fig. s18b: it is evident that a desorption time of 30 minutes is a good compromise and allows to maximize the SDWP, at least theoretically. Note that, repeating the same simulation using the standard LDF model instead of the modified LDFDw, the maximum would be slightly shifted down ($SDWP = 2.36\ m^3/day/ton$) and to the left ($t_{Des} = 21\ min$), but the results and considerations are qualitatively the same. All the simulations have been carried out with a fixed adsorption time of 30 min (the same as in the experimental campaign); in case the adsorption time increases, the maximum is shifted to the right (higher adsorption times require higher desorption times in order to restore the same water content in the material).

Thanks to the experimental data available, it is possible to plot in comparison the actual SDWP of the CaAlg when used in the desalination unit. This is shown in Fig. s18b in dotted lines, both considering the average on all the cycles of the test (black line, with bars for $\pm$ one standard deviation) and considering only the last cycle (green line); the latter choice might result in a more reliable approximation, since the initial cycles might be affected by the starting daily uptake. The two curves are slightly different, but in both cases there is a maximum for a desorption time around 45-60 minutes. Two considerations follow:

- the experimental optimal SDWP is approximately 100% larger than the theoretical one. This can be in part explained by the fact that the assumed value $w_{des,eq}$ for desorption might be overestimated (details are provided below), and in part by the fact that the diffusivities used in the model are obtained in conditions different from the experiments: they are derived from the tests with the ProUmid analyser, working under positive pressure. In the real desalination unit, though, the adsorption and desorption processes happen under vacuum: this might contribute to increase the effective diffusivity, since the water molecules in the chamber are not hindered by gas molecules in reaching or leaving the sorbent. By repeating the simulation assuming 100% larger diffusivities, the maximum SDWP increases up to the value of $6.02\ m^3/day/ton$ (magenta line in Fig. s18b), similar to the experimental one. The latter curve is reported in the main text, Fig. 4b.
- the desorption time at which the experimental optimal SDWP is found is larger, being the whole curve shifted to the right. This can be explained by the fact that in a real machine the material is not immediately brought to the ideal set conditions: the high thermal inertia of the system, as well as the difference existing in the heat exchanger between the feedback temperature T1 of the water in the pipes and the actual temperature of the material, suggest that the material desorbed at an effective temperature lower, in average, than the nominal one. Also, most probably the material temperature is not uniform in the exchanger, being greater around the centre of the fins where the copper pipes pass, and lower close to the exchanger sides.

An equilibrium value during desorption of $w_{des,eq} = 0.00\ g/g$ is clearly not the actual value, but no information is available for the material sorption properties at 60°C. Nevertheless, it was simulated that

a different value does not affect the shape of the result nor the qualitative discussion that followed. Indeed:

- by repeating the same simulation using a larger $w_{des,eq}$, the maximum is still found at the same optimal desorption time, only lower (e.g., with $w_{des,eq} = +0.20\ g/g$, the maximum is at $t_{Des} = 30\ min$ and $SDWP = 2.30\ m^3/day/ton$);
- on the other hand, using a lower $w_{des,eq}$, the maximum is still found at the same desorption time, only higher (e.g., with $w_{des,eq} = -0.20\ g/g$, the maximum is at $t_{Des} = 30\ min$ and $SDWP = 3.91\ m^3/day/ton$).

Note S13 – Replacement of the material in the desalination unit

The replacement of the material in the desalination unit (which took place before test #1 and before test #7) requires the following steps:

1) release the vacuum from the machine;
2) remove the exchanger from the adsorber vessel;
3) unscrew a protection mesh preventing the material from leaving the space between the fins (Fig. s19);
4) remove the previous material;
5) fill with the new material;
6) screw the protection mesh in place again;
7) insert the exchanger in place;
8) heat up the adsorber to 75°C using the external orange circuit;
9) restore vacuum in the chamber (a 250W double-stage vacuum pump has been used for the purpose).

At the end of the procedure, after the adsorber cools down to environmental temperature, the pressure sensor measures ~0.5 mbar of residual gas (air + vapor) in the chamber. The first 2-3 cycles run after the machine is opened are not considered in the experimental campaign, since the results would be affected by a vacuum level which is not reachable again during the normal operation of the machine.

Figure s19: Detail of the fine mesh used to cover the exchanger sides, keeping the material inside. A ruler (in cm) is placed for reference.

Note S14 – Use of the vacuum pump during a test

The step of opening valve V3 for one further minute with the vacuum pump on was introduced when it was noticed that the desalination unit offers a limitation in the vapor mobility due to the high pressure drops introduced by the portion of circuit between the EV tank and the adsorber (including valve V2). The small diameter of the connection makes the vapor movement difficult and, if the pressure close to the inlet of the adsorber chamber is high, there might be no vapor passage or even backflow from the adsorber chamber to the EV tank. In principle this step would not be necessary, since the adsorbent material itself is already able to reduce the pressure in the chamber below the saturation pressure in the EV tank, but it was included as a standard step to have repeatability among cycles. The same was included for all tests and all cycles, both for CaAlg and mesoporous silica-gel.

The work introduced in the machine by powering the vacuum pump during the cycle (approximately 4 Wh) is negligible with respect to the thermal energy exchanged with the material (100÷300 Wh) and comparable with the electronic consumptions of the microcontroller during the cycle (approximately 5 Wh).

Note S15 – Choice of best-fitting equilibrium model

The choice of the GAB model to best-fit experimental data and estimate the enthalpy of adsorption is justified by the isotherm type ("S-shape", corresponding to type-II according to the ISO classification) and the lowest error made in best-fitting data (see Fig. s20).

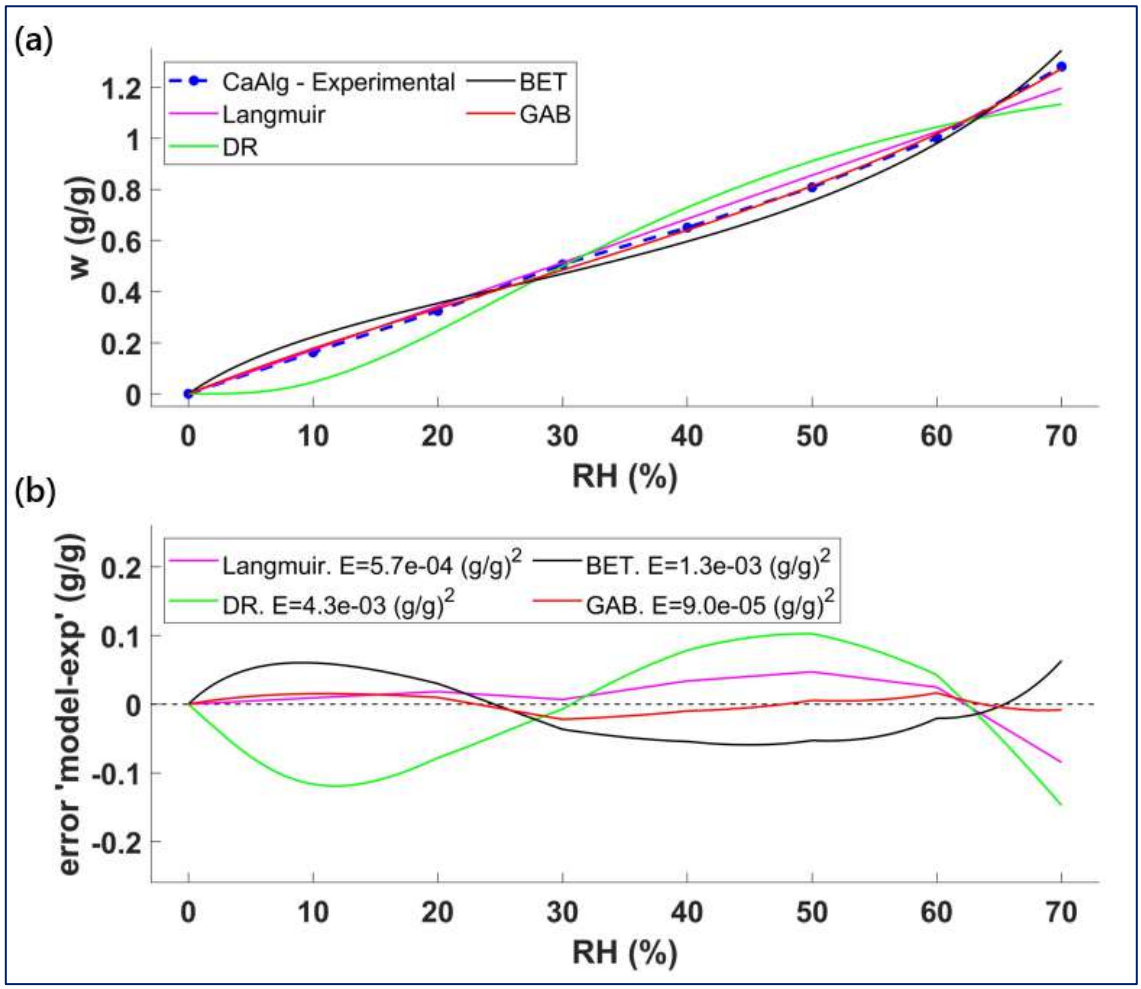

Figure s20: (a) CaAlg adsorption isotherm best-fitted by equilibrium models Langmuir, Dubinin-Radushkevich (DR) [S 20], *BET, GAB. (b) Errors made by each model over experimental data. In the legend, we report the errors "E", evaluated as the definite integral over RH of the square of the difference between model and data. A lower value for "E" is associated with a better-fitting model.*

Note S16 – Dependence of CaAlg beads volume of RH

Based on the ProUmid camera pictures taken during the construction of the isotherm at 30°C on CaAlg, we estimated how the diameter of the hydrogel beads changes with the increase in vapor pressure.

We randomly selected 10 beads in the aluminium dish containing the sample under test. Per each bead, we drew three diameters and averaged them, to determine an equivalent bead diameter (this is a simplified way to account for non-perfect spherical shape). We report in fig. s21 (blue dotted line) the average and standard deviation of the equivalent bead diameter as measured over the 10 selected beads. The same process was repeated at each relative humidity between 10% and 70%.

Comparing the conditions at RH=10% and RH=70%, we observe a change in CaAlg diameter of 22.6% (corresponding to a change in volume of 84%, assuming spherical shape). This is important to consider for the heat exchanger design. In our case, we used a finned coil heat exchanger with a distance between fins of 3 mm, which is sufficient to host our CaAlg beads in equilibrium at RH=70% (the maximum observed diameter does not exceed 2 mm).

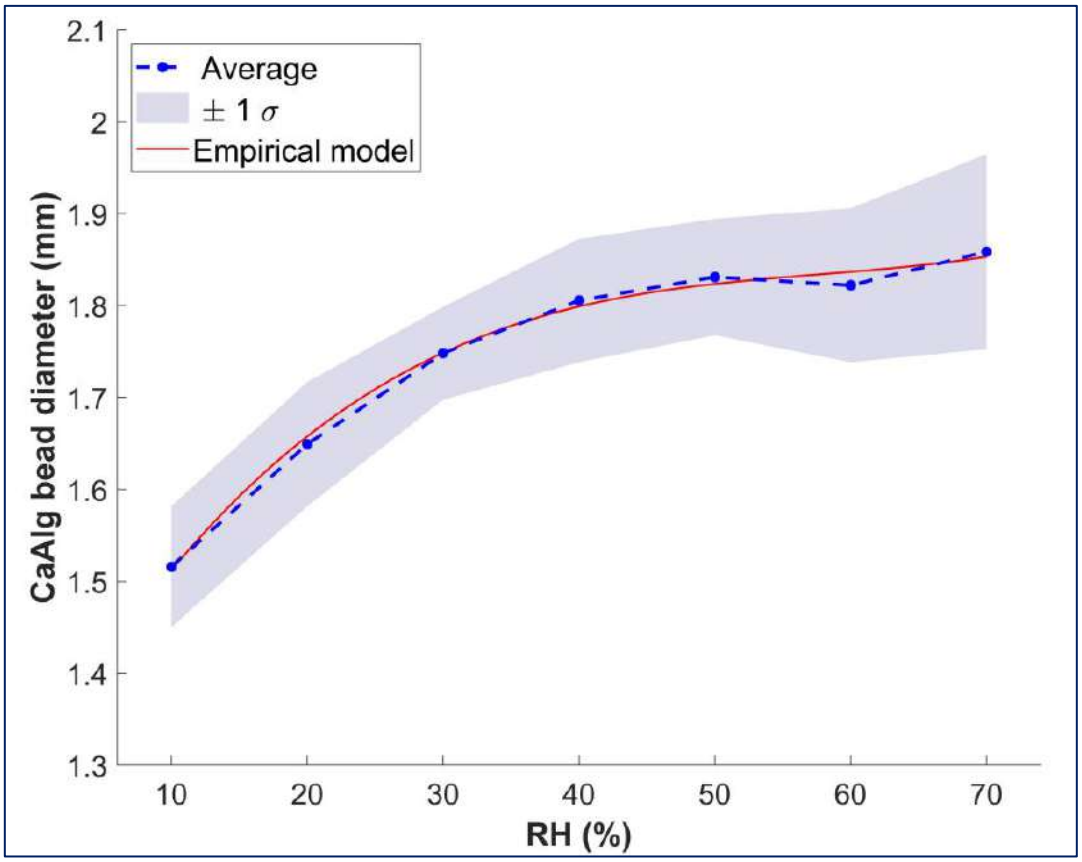

Figure s21: Relationship between equilibrium RH and CaAlg beads diameter, at T=30°C. The blue dotted line connects the experimental measurements, each taken as average over 10 beads (per each bead, three diameters were averaged, for a total of 30 measurements per each RH). The blue background area encloses ± one standard deviation calculated on the 10 beads considered at each RH. The red curve corresponds to the best-fitting cubic curve: $D(RH)=2.41\cdot(RH/100)^3 - 4.19\cdot(RH/100)^2 + 2.55\cdot(RH/100) + 1.30$.

Note S17 – Dependence of SDWP on diameter of produced beads

In this work, we have produced CaAlg beads with dry diameter of approximately 1.5 mm. We provide here a simplified theoretical analysis which explores how the SDWP would change if the CaAlg beads were produced in different size. As an example, we see that decreasing the beads diameter to 1.0 mm should approximately double the expected SDWP: this goes in the direction of further increasing the water production achievable with CaAlg. Future research should validate this experimentally.

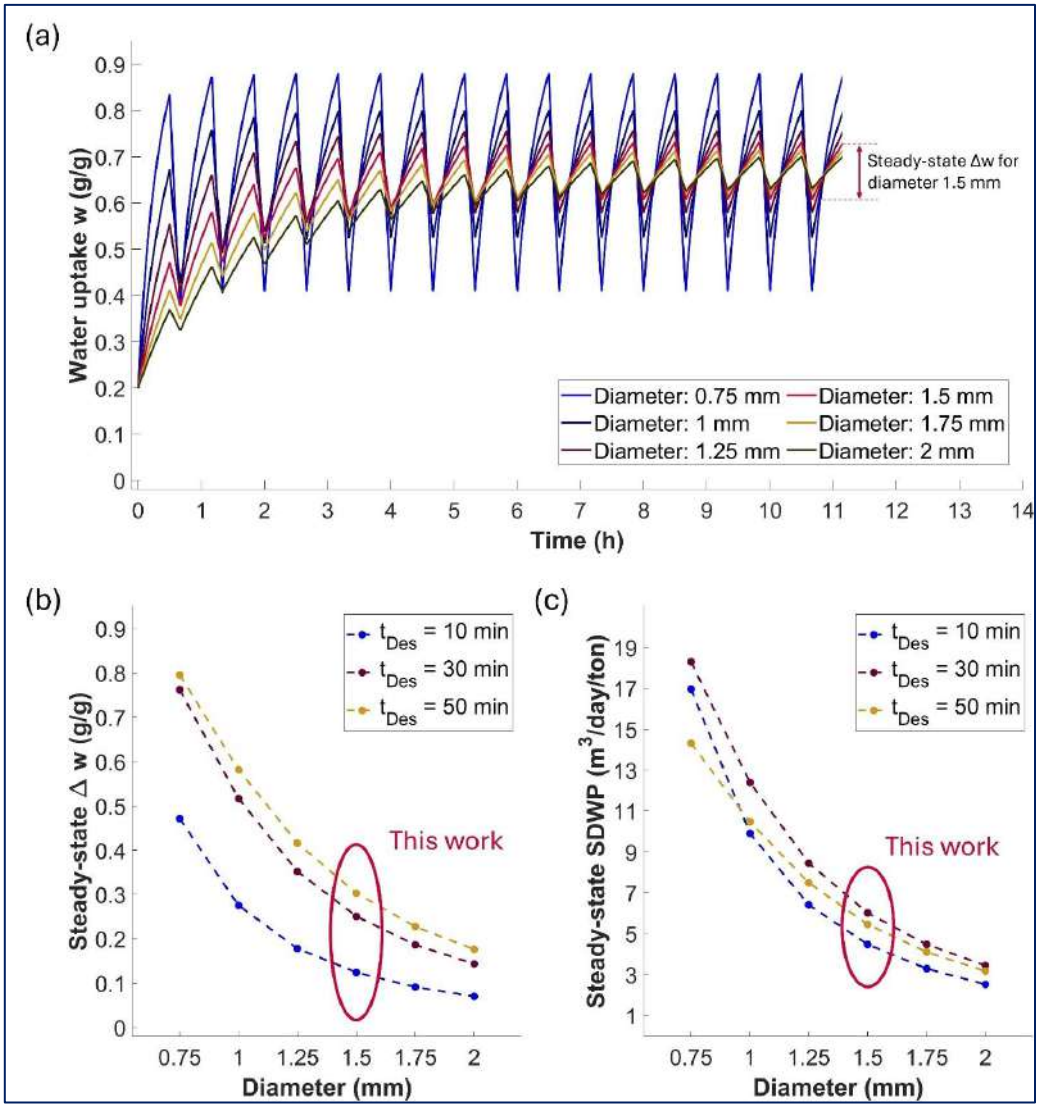

Figure s22: (a) Theoretical change in water uptake over time, as resulting from the alternation of adsorption and desorption transients, at fixed adsorption time (30 min) and desorption time (10 min). Each curve corresponds to a different diameter for the CaAlg beads. The simulations start from an initial uptake of 0.2 g/g, and continue until steady-state condition (that we defined as when the difference between subsequent uptakes at the end of adsorption is ≤ 1 mg/g). For the simulation, we used model LDFDw, with the best-fitted parameters derived in this work and used for the analysis in fig. 4b (in the main text): $Da_{30°C}=8.88\cdot10^{-12}$ m²/s, $Da_{60°C}=2\cdot8.88\cdot10^{-12}$ m²/s, $Db_{30°C}=-4.60\cdot10^{-12}$ m²/s, $Db_{60°C}=-2\cdot4.60\cdot10^{-12}$ m²/s, $w_{eq,Ads}$ = 1.12 g/g, $w_{eq,Des}$=0 g/g. (b) The steady-state uptake difference from *a*, is plotted against the beads diameter. Each curve corresponds to the Δw resulting from running the simulation in *a* with constant adsorption time (30 min) and different desorption times (10, 30, 50 min). (c) Theoretical SDWP resulting by dividing the steady-state Δw from *b* by the cycle time (that is, sum of adsorption and desorption times).

References

S1. Thu, K., Ng, K. C., Saha, B. B., Chakraborty, A. & Koyama, S., Operational strategy of adsorption desalination systems. *International Journal of Heat and Mass Transfer* **52** (7), 1811-1816 (2008).

S2. Ng, K., Thu, K., Chakraborty, A., Saha, B. & Chun, W., Solar-assisted dual-effect adsorption cycle for the production of cooling effect and potable water. *International Journal of Low-Carbon Technologies* **4**, 61-67 (2009).

S3. Alsaman, A. S., Askalany, A. A., Harby, K. & Ahmed, M. S., Performance evaluation of a solar-driven adsorption desalination-cooling system. *Energy* **128**, 196-207 (2017).

S4. Ghazy, M. *et al.*, Solar powered adsorption desalination system employing CPO-27(Ni). *Journal of Energy Storage* **53**, 105174 (2022).

S5. Elsayed, E., AL-Dadah, R., Mahmoud, S., Anderson, P. & Elsayed, A., Experimental testing of aluminium fumarate MOF for adsorption desalination. *Desalination* **475**, 114170 (2020).

S6. Olkis, C., Brandani, S. & Santori, G., Design and experimental study of a small scale adsorption desalinator. *Applied Energy* **253**, 113584 (2019).

S7. Ibrahim, A., Elsheniti, M. B., AL-Dadah, R., Mahmoud, S. & Solmaz, İ., Numerical and experimental investigation of multiple heat exchanger modules in cooling and desalination adsorption system using metal organic framework. *Energy Conversion and Management* **251**, 114924 (2022).

S8. Mohd Abdullah Khan & al, Experimental evaluation of Adsorption Heat for Water vapour/Silica gel pair for chiller application. *Applied Thermal Engineering* (2024).

S9. Palomba, V. *et al.*, Experimental proof of a thermal system for cooling and storage applications employing cacl2/silica gel composite adsorbent. *Energy Conversion and Management* **341**, 120072 (2025).

S10. Frank Dorinel Solefack Feudjio & al, Tunable water vapor adsorption properties on ion exchange microporous zeolite Na-X derived from natural kaolin. *Inorganic Chemistry Communications* (2025).

S11. Marina V. Solovyeva & al, Water Vapor Adsorption on CAU-10-X: Effect of Functional Groups on Adsorption Equilibrium and Mechanisms. *Langmuir* (2021).

S12. Nasreen & Ijmtst, Ocean Salinity. *International Journal for Modern Trends in Science and Technology* **8**, 296-302 (2022).

S13. Gentile, V., Calò, M., Bozlar, M., Simonetti, M. & Meggers, F., Water vapor mass transfer in alginate–graphite bio-based hydrogel for atmospheric water harvesting. *International Journal of Heat and Mass Transfer* **219** (2024).

S14. Glueckauf, E., Theory of chromatography. Part 9. The “theoretical plate” concept in column separations. *Trans. Faraday Soc.* **51**, 34-44 (1955).

S15. Aristov, Y., Tokarev, M., Freni, A., Glaznev, I. & Restuccia, G., Kinetics of water adsorption on silica Fuji Davison RD. *Microporous and Mesoporous Materials - MICROPOROUS MESOPOROUS MAT* **96**, 65-71 (2006).

S16. Gentile, V., Innovative Adsorption Heat Exchangers for Desiccant Cooling and Atmospheric Water Harvesting (2020).

S17. Sikorski, P. & al, Evidence for Egg-Box-Compatible Interactions in Calcium–Alginate Gels from Fiber X-ray Diffraction. *Biomacromolecules* (2007).

S18. Fang, Y. & al, Multiple Steps and Critical Behaviors of the Binding of Calcium to Alginate. *The Journal of Physical Chemistry B* (2007).

S19. Li, L. & al, Reexamining the Egg-Box Model in Calcium–Alginate Gels with X-ray Diffraction. *Biomacromolecules* (2007).

S20. Lihua Hu & al, Facile preparation of watersoluble hyperbranched polyamine functionalized multiwalled carbon nanotubes for high-efficiency organic dye removal from aqueous solution. *Scientific Reports* (2017).